



Overview of SLOPE I and II campaigns: aerosol properties retrieved with lidar and sun-sky photometer measurements

5 Jose Antonio Benavent-Oltra^{1,2}, Juan Andrés Casquero-Vera^{1,2}, Roberto Román³, Hassan Lyamani^{1,2}, Daniel Pérez-Ramírez^{1,2}, María José Granados-Muñoz^{1,2}, Milagros Herrera⁴, Alberto Cazorla^{1,2}, Gloria Titos^{1,2}, Pablo Ortiz-Amezcu^{1,2}, Andrés Esteban Bedoya-Velásquez^{2,5}, Gregori de Arruda Moreira^{2,6}, Noemí Pérez⁷, Andrés Alastuey⁷, Oleg Dubovik⁴, Juan Luis Guerrero-Rascado^{1,2}, Francisco José Olmo-Reyes^{1,2} and Lucas Alados-Arboledas^{1,2}

¹Department of Applied Physics, Universidad de Granada, Granada, Spain.

²Andalusian Institute for Earth System Research, IISTA-CEAMA, Granada, Spain.

10 ³Group of Atmospheric Optics (GOA-UVa), Universidad de Valladolid, Valladolid, Spain.

⁴Laboratoire d'Optique Atmosphérique (LOA), UMR8518 CNRS, Université de Lille, Villeneuve D'ASCQ, France.

⁵The French Aeospace Lab, ONERA, Toulouse, France.

⁶Federal Institute of São Paulo (IFSP), São Paulo, Brazil.

15 ⁷Institute of Environmental Assessment and Water Research (IDAEA), CSIC, Barcelona, Spain.

Correspondence to: Jose Antonio Benavent-Oltra (jbenavent@ugr.es)

Abstract. The Sierra Nevada Lidar aerosol Profiling Experiment I and II (SLOPE I and II) campaigns were intended to determine the vertical structure of the aerosol by remote sensing instruments and test the various retrieval schemes for obtaining aerosol microphysical and optical properties with in-situ measurements. These campaigns deployed a set of in-situ and remote sensing instruments at the stations include in AGORA observatory (Andalusian Global ObseRvatory of the Atmosphere) in the Granada area (Spain) along summer in 2016 and 2017. In this work, using the in-situ measurements performed at a high-altitude station, Sierra Nevada station, and airborne flights, we evaluate the retrievals of aerosol properties by GRASP code (Generalized Retrieval of Atmosphere and Surface Properties) combining lidar and sun-sky photometer measurements. Besides, we show an overview of aerosol properties retrieved by GRASP during SLOPE I and II campaigns. We evaluate the GRASP retrievals of total aerosol volume concentration (discerning between fine and coarse modes), extinction and scattering coefficients, and for the first time we present an evaluation of absorption coefficient.

30 The statistical analysis of the aerosol optical and microphysical properties, both column-integrated and vertically-resolved, from May to July 2016 and 2017 shows a large variability in aerosol load and types. The results show a strong predominance of desert dust particles due to the North African intrusions. The vertically-resolved analysis denotes a decay of the atmospheric aerosols with altitude up to 5 km a.s.l. Finally, two events of desert dust and biomass burning were used to show the high potential of GRASP to retrieve and study the aerosol properties profiles such as absorption coefficient and single scattering albedo for



different aerosol types. The aerosol properties retrieved by GRASP show good agreement with simultaneous in situ measurements performed at Sierra Nevada Station (SNS) in Granada. In general, GRASP overestimates the in situ data at SNS with a mean difference lower than 6 $\mu\text{m}^3/\text{cm}^3$ for volume concentration, 11 Mm^{-1} and 2 Mm^{-1} for scattering and absorption coefficient. On the other hand, the comparison of GRASP with airborne measurements also shows an overestimation with mean absolute differences of $14 \pm 10 \text{ Mm}^{-1}$ and $1.2 \pm 1.2 \text{ Mm}^{-1}$ for scattering and absorption coefficients, showing a better agreement for absorption (scattering) coefficient with higher (lower) aerosol optical depth. The potentiality of GRASP showed in this study will contribute to enhancing the representativeness of the aerosol vertical distribution and provide information for satellite and global model evaluation.

1. Introduction

The characterization of atmospheric aerosol optical and microphysical properties is difficult due to their high spatial and temporal variability in the atmosphere. These together with the complexity of the aerosol-radiation interaction (scattering and absorbing incident solar and outgoing thermal radiation) and the cloud-aerosol interaction (modifying cloud properties), results in a large uncertainty in the radiative forcing of climate due to aerosols (IPCC, 2013).

During the last decades, a good number of field campaigns has been carried out for studying atmospheric aerosol properties (e.g., Tanré et al., 2003; Mallet et al., 2016; Veselovskii et al., 2016; Vandenbussche et al., 2020) using observatories with in-situ measurements and included in global networks, based on passive and active remote sensing instruments, such as AERosol RObotic NETwork (AERONET; Holben et al., 1998) and European Aerosol Research Lidar NETwork (EARLINET; Pappalardo et al., 2014). On the one hand, the in-situ ground-based observatories only represent limited atmospheric sample in the layer closest to the surface. The passive remote sensing instruments, such as sun-sky photometers or satellites provide aerosol properties in entire atmospheric column, while have very limited information about variations within the column. Hence, vertically-resolved aerosol observations are needed to discern between the different aerosol layers and to study their radiative properties. In these regards, the lidar systems are used for aerosol optical and microphysical properties profiling. Advanced lidar systems have information on the backscatter elastic and inelastic signals which allow the retrieval of the backscatter coefficient (β) profiles by the Klett-Fernald method (Fernald et al., 1972; Fernald, 1984; Klett, 1981, 1985) and the extinction coefficient (α) profiles by the Raman technique (e.g. Ansmann et al., 1992; Whiteman et al., 1992). These measurements allow retrieving the particle vertical



70 microphysical properties by inversion algorithms using the $3\beta + 2\alpha$ configuration (e.g. Müller et al., 1999; Böckmann, 2001; Veselovskii et al., 2002).

The main drawback of these algorithms is the scarcity of Raman lidar measurements during the daytime that represents a limitation to the retrieval of the extinction coefficient data (Veselovskii et al., 2015; Ortiz Amezcua et al., 2020). As an alternative, during the last years,
75 several synergetic retrievals algorithms have been developed to retrieve aerosol optical and microphysical properties combining data from sun-sky photometers and backscatter lidar measurements such as LIRIC (Lidar-Radiometer Inversion Code) by Chaikovskiy et al. (2008, 2016, Granados-Muñoz et al., 2020) and GARRLiC (Generalized Aerosol Retrieval from Radiometer and Lidar Combined data) by Lopatin et al. (2013). One of the most popular
80 advanced inversion algorithms is the Generalized Retrieval of Atmosphere and Surface Properties code (GRASP; Dubovik et al., 2011, 2014). It should be noted here that GARRLiC is a branch of GRASP. The versatility of GRASP allows the retrieval of aerosol vertical and surface properties combining different types of measurements, such as sun-photometers, lidar, ceilometers, satellite, sky-cameras, nephelometers, etc. (e. g. Lopatin et al., 2013; Espinosa et al., 2017; Román et al., 2017; Torres et al., 2017; Benavent-Oltra et al., 2017; Titos et al., 2019
85 Herreras et al., 2019; Dubovik et al., 2019). In addition, GRASP retrievals have been used to evaluate forecast models, as constrains for global models and as inputs for radiative transfer models (e.g. Tsekeri et al., 2017; Chen et al., 2018, 2019; Granados-Muñoz et al., 2019). It is important to explore the potential of this kind of algorithms by applying them to different input
90 data and for different atmospheric conditions. In these regards, the extensive measurement dataset obtained during Sierra Nevada Lidar aerOsol Profiling Experiment I and II (SLOPE I and SLOPE II) campaigns in May, June and July 2016 and 2017, respectively, allow an evaluation of the atmospheric aerosol properties retrieved by GRASP code combining lidar and sun-sky photometer measurements. This database was successfully utilized in several
95 previous studies of the atmospheric aerosol (e.g. de Arruda Moreira et al., 2018, 2019; Bedoya-Velásquez et al., 2018; Horvath et al., 2018; Casquero-Vera et al., 2020).

The main objective of this work is to provide an overview of the aerosol optical and microphysical properties during SLOPE I and II campaigns using the GRASP code. We check the GRASP retrievals versus in-situ measurements performed at the Sierra Nevada Station
100 (SNS, Spain; 2500 m a.s.l.) and instrumented flights. In contrast to previous studies by Román et al. (2018) and Titos et al. (2019), which mainly evaluated long-term vertical profiles retrieved by GRASP combining sun-sky photometer and ceilometer measurements here, for



the first time, we study aerosol properties such as absorption coefficients and volume concentration for fine and coarse modes, separately. In addition, a statistical analysis of both total column and vertically-resolved aerosol properties is performed, and two extreme events of desert dust and biomass burning are evaluated.

2. Sites and measurements

The SLOPE I and II campaigns took place in Granada (Spain) during the summers of 2016 and 2017 and were designed to determine the vertical structure of the aerosol by remote sensing instruments through the application of various retrieval schemes for obtaining aerosol microphysical and optical properties. The main objective of this campaign was to perform a closure study by comparing remote sensing system retrievals of atmospheric aerosol properties with various in-situ measurements (Román et al., 2017; Benavent-Oltra et al., 2019). The study area typically presents very variable aerosol loads and type, with large presence of anthropogenic aerosols mainly in winter (e.g., Lyamani et al., 2010; del Aguila et al., 2018; Casquero-Vera et al., 2021) and frequent Saharan dust intrusions (e.g., Perez-Ramirez et al., 2012; Valenzuela et al., 2012) and primary aerosol associated to the local phenology (Cariñanos et al., 2020). The region is often affected by episodes of aerosol stagnation due to its complex geography (e.g., Lyamani et al., 2010), while Atlantic air masses are usually responsible for cleaning the atmosphere (Perez-Ramirez et al., 2016).

During SLOPE I and II the instrumentation was deployed at the three stations of the AGORA (Andalusian Global ObseRvatory of the Atmosphere) observatory. The main station of AGORA is in the Andalusian Institute for Earth System Research / IISTA-CEAMA (UGR; 37.16° N, 3.61° W; 680 m a.s.l.) in the city of Granada. UGR station operates many remote sensing and in-situ instrumentation, mostly in the framework of ACTRIS (Aerosols, Clouds, and Trace gases Research InfraStructure Network, <https://www.actris.eu/default.aspx>) research infrastructure. The other two stations of AGORA observatory are in the Sierra Nevada Mountain range: Cerro Poyos (CP; 37.11° N, 3.49° W; 1820 m a.s.l.) and Sierra Nevada Station (SNS; 37.10° N, 3.39° W, 2500 m a.s.l.). SNS is located ~20 km southeast of Granada city and 1.8 km above UGR station (see Figure 1 in Herreras et al., 2019 for details). During SLOPE field campaigns, a large set of in-situ instrumentation was deployed at SNS station and on-board the Partenavia P68 airplane. The in-situ measurements allow the validation of aerosol optical and microphysical properties obtained by remote sensing techniques at the UGR station. Table 1 summarizes the main instrumentation operating in UGR, SNS and on-board the airplane.



[Table 1]

2.1. Remote sensing instrumentation

The UGR station is equipped with a multi-wavelength Raman lidar system (LR331D400, Raymetrics S.A.), which is included in EARLINET since 2005 and contributes to the ACTRIS research infrastructure. This instrument is composed of a Nd:YAG pulsed laser that emits at 1064 nm (110 mJ per pulse), 532 nm (65 mJ per pulse) and 355 nm (60 mJ per pulse). The detection branch has seven channels: four to measure the backscattered light at 355, 532 (parallel and perpendicular components) and 1064 nm; two channels at 353.9 and 530.2 nm (387 and 607 nm until December 2016; Ortiz-Amezcuca et al., 2020) for the detection of Raman scattering from N₂, and one channel to detect the water vapour Raman scattering at 408 nm. More information of this instrument can be found in Guerrero-Rascado et al. (2008, 2009) and Ortiz-Amezcuca et al. (2020).

Each station of AGORA is equipped with a sun-sky photometer CE-318 (Cimel Electronique S.A.S.) that operate in frame of the AERONET network. This instrument performs measurements of sun direct irradiance, which is used to derive the aerosol optical depth (AOD) usually at 340, 380, 440, 500, 675, 870 and 1020 nm, and sky radiance in almucantar configuration at 440, 675, 870 and 1020 nm. The instruments at UGR and SNS during SLOPE I and II were sun-sky-lunar photometer Cimel CE318-T, which also perform lunar direct irradiance measurements to retrieve the AOD during night-time between the first and third Moon quarters (e.g., Barreto et al. 2016, 2019, Román et al., 2020). In this work, we used AERONET Version 3 Level 1.5 (cloud-screened) data (e.g., Giles et al., 2019; Sinyuk et al., 2020).

The ground-based MWR (RPG-HATPRO G2, Radiometer physics GmbH) located at UGR station as part of the MWRnet (Rose et al., 2005; Caumont et al., 2016), is used here for retrieving temperature profiles. MWR is a passive remote sensor that performs measures unattended of the brightness temperatures of oxygen and water vapor in the atmosphere. The oxygen is measured in the K-band (51-58 GHz) and the water vapor in the V-band from 22 to 31 GHz with a radiometric resolution between 0.3 and 0.4 rms errors at 1.0 s integration time. The retrievals of temperature profiles from the measured brightness temperatures are performed using a standard feed forward neural network (Rose et al., 2005). A detailed description of this system can be found in Navas-Guzmán et al. (2014) and Bedoya et al. (2018, 2019).



2.2. In-situ instrumentation

The integrating nephelometer (model TSI 3563) at SNS measures the particle light scattering coefficient (σ_{sca}) at three wavelengths (450, 550 and 700 nm) with 1-min temporal resolution. The aerosol flow in the nephelometer was set to 30 lpm. The nephelometer measurements are within the angular range 7-170°, so the data were corrected for truncation and non-Lambertian illumination errors (Anderson and Ogren, 1998). The Aethalometer AE-33 (Magee Scientific Company, 206 Berkeley, USA) is based on filter technique and provides aerosol absorption coefficient (σ_{abs}) at seven wavelengths (370, 470, 520, 590, 660, 880 and 950 nm). The aethalometer was intercompared with other similar systems during the ACTRIS inter-comparison (ACTRIS 2 Absorption Photometer Workshop, September 2015, Leipzig, Germany), which assures the data quality. The combination of integrating nephelometer and aethalometer data allows the calculation of the aerosol extinction coefficients (α).

The Scanning Mobility Particle Sizer (SMPS) composed of an Electrostatic Classifier (TSI Mod. 3082) and a Condensation Particle Counter (CPC; TSI Mod. 3772), provides the sub-micron particle number size distribution within the 12–615 nm particle mobility diameter range with 5-min temporal resolution. SMPS data have been corrected of internal diffusion losses and multiple charges by AIM software (version 10.2.0, TSI, Inc., St Paul MN, USA). The SMPS measurements followed ACTRIS and GAW recommendations (Wiedensohler et al., 2012, 2018) and high-quality data were guaranteed after the successful participation of the instrument in the ACTRIS inter-comparisons workshops (TROPOS, Leipzig, Germany) and in-situ intercomparison (ACTRIS Round Robin Tour). The Aerodynamic Particle Sizer (APS; TSI Mod. 3321) provides the coarse particle number size distribution within the 0.5–20 μm aerodynamic diameter range. The APS also measures number aerosol concentrations up to 1000 particles·cm⁻³ with coincidence errors inferior to 5% and 10% at 0.5 and 10 μm diameters, respectively. By the combination of SMPS and APS measurements, total aerosol volume concentrations were obtained in the 0.05–10 μm radius range with 5-min time resolution. To that end, Q-value=1 has been assumed for conversion from aerodynamic to mobility size distribution (Sorribas et al., 2015).

2.3. Aircraft instrumentation

During the campaigns, dedicated flights with an airplane (Piper PA 34 Seneca) equipped with in-situ instrumentation were carried out over the study area between 15th and 18th June 2016 for SLOPE I, and between 21st and 24th June 2017 for SLOPE II campaigns. The aircraft campaigns consisted of 3 flights each year. Figure 1 shows the spiral trajectories of one flight,



each flight consisted of several ascending and descending spiral profiles centred on the location of the UGR station. The radius of the spirals were about 500 meters. On each flight, only ascending profiles were used in the following analysis. To avoid the potential partial sampling of the exhaust of the aircraft, the descending profiles were performed on a different location.

205

[Figure 1]

Air flows to the instruments through a near-isokinetic isoaxial inlet designed by Aerosol d.o.o. (www.aerosol.si) at a flow rate of 10 lpm. The main flow is divided by two flow splitters that divide de sampled air among the instruments. Yus-Díez et al. (2020) reported minimal losses in the inlet system for small particles, while larger differences were observed for particles with diameter $>4\text{-}5\ \mu\text{m}$. The Ecotech Aurora nephelometer is an integrating nephelometer that measures the particle light scattering coefficient at three wavelengths (450, 525 and 635 nm) with a time resolution of 10 seconds. This instrument measures the scattering coefficient in the angular range $10\text{-}170^\circ$, and the correction of Müller et al. (2011) was used to account for the angular truncation errors. The Aethalometer AVIO AE33 (Aerosol d.o.o.) is the aircraft version of the Aethalometer AE-33 described above. Using the same measurement principle (Drinovec et al., 2015) it provides particle absorption coefficients at seven wavelengths (370, 470, 520, 590, 660, 880 and 950 nm) with a time resolution of 1 second. The position of the aircraft was tracked using a GPS and all instruments on-board the aircraft were time-synchronized. Further information on the aircraft instrumentation can be found in Yus-Díez et al. (2020).

210

215

220

3. Methodology

In this work, we use the GRASP algorithm following the scheme proposed by Lopatin et al. (2013), which combines lidar and sun-sky photometer measurements to retrieve the optical and microphysical properties of aerosol particles. This scheme uses normalized backscattered range corrected signal at 355, 532 and 1064 nm and the AOD and sky radiance (almucantar scan) both at 440, 675, 870 and 1020 nm from AERONET version 3 level 1.5. It should be noted that GRASP retrievals were performed during daytime with solar zenith angles larger than 40° and clear-sky conditions. This configuration of GRASP allows the retrieval of aerosol properties for both fine (radii range $0.05\text{ to }0.576\ \mu\text{m}$) and coarse (radii range $0.33\text{ to }15\ \mu\text{m}$) modes separately, the complex refractive index, single-scattering albedo (SSA) and lidar ratio (LR). Besides, GRASP provides vertical concentration of fine and coarse mode separately, and the vertically-resolved profiles of the extinction, absorption and scattering coefficients, SSA, LR,

225

230



235 Ångström exponent of absorption (AAE) and scattering (SAE). Previous evaluations of GRASP with LIRIC, Klett-Fernald method and in-situ data, showed differences lower than 30% for the backscatter coefficient and 10–20% for the extinction coefficient and the volume concentration (Lopatin et al., 2013; Benavent-Oltra et al., 2017; Tsekeri et al., 2017).

Individual GRASP retrievals are performed for each sky radiance almucantar sequence available from AERONET with correlative lidar measurements in a ± 15 min time window. Specifically, the normalized lidar range corrected signal profile used in each retrieval is
240 previously 30-min averaged and computed for 60 log-spaced heights between a minimum and maximum heights as proposed by Lopatin et al. (2013). Here, the minimum height has been chosen as 400 m above the ground to minimize the effect of incomplete overlap and maximum height as 6000 m above the ground to have better signal-to-noise ratio. This GRASP configuration is described in detail in Benavent-Oltra et al. (2019). The data used in this study
245 were recorded between May and July of 2016 and 2017 with 286 retrievals in 69 days that passed the filter imposed to the inversion process (relative residual $< 15\%$; Torres et al., 2017).

3.1. Aircraft data

In order to make comparable the profiles from the aircraft data and the remote sensing retrievals, there are some corrections to consider. Remote sensing data are provided at ambient
250 conditions (temperature and pressure), but the aircraft data is registered at different conditions. Nephelometer data from the aircraft were recorded at cabin temperature and ambient pressure, and aethalometer data were registered at 0°C and 1013.25 hPa. The cabin temperature used was the nephelometer sampling temperature (T_s), i.e. temperature inside the nephelometer, and the profile atmospheric pressure used was the nephelometer pressure sensor (P_s). The cabin on the
255 aircraft was not pressurize so the pressure inside the nephelometer can be consider the outside pressure. The aircraft did not register the outside temperature, so an external source of temperature profile was required. We used a temperature profile from a microwave radiometer MWR (T_{mwr}) as described in section 2.1., using an average profile during the time of the entire aircraft profile and interpolated to the exact altitudes of the aircraft profile.

260 Aircraft profiles show some noise, especially at higher altitudes, so a convolution with a mean filter was applied to the aircraft in-situ data in order to smooth the profiles. We observed that using 100 meters for the nephelometer and 200 meters for the aethalometer data in the vertical profiles reduced noise while preserving the profile features. Finally, Aurora



nephelometer wavelengths were converted to the TSI wavelengths using the Ångström
265 exponent law to make the aircraft and ground based in-situ data comparable.

4. Results

4.1. Evaluation of GRASP retrievals versus in-situ data

4.1.1. At high mountain station

For the inter-comparison between GRASP retrievals and SNS in-situ data, we selected the in-
270 situ measurements averaged in ± 15 min around the GRASP retrieval time and the 400 m
averaged data of GRASP retrieval profile at 2500 m a.s.l. (SNS altitude). Therefore, the results
and discussion about the comparison between GRASP and SNS in-situ measurements are
referred exclusively to this height range.

Figure 2 shows the aerosol total (VC_T), fine mode (VC_F) and coarse mode (VC_C)
275 volume concentration retrieved by GRASP versus those measured with in-situ instruments at
SNS. The aerosol volume concentrations at SNS were calculated for fine and coarse mode in
the 0.05 – 0.5 and 0.5 – 10 μm radius size range for fine and coarse modes, respectively. Due
to the sensibility of linear regression to outliers, VC_T concentrations larger than 190 $\mu\text{m}^3/\text{cm}^3$
(99th percentile) and their corresponding fine and coarse data have been excluded in this
280 analysis. In general, volume concentrations retrieved by GRASP code shows good correlation
with SNS measurements with correlation coefficients (R) of 0.58, 0.83 and 0.80 for fine, coarse
and total volume concentrations, respectively. The results show that GRASP retrievals
overestimate in-situ measurements with a mean difference (\pm standard deviation) of 4 ± 4
 $\mu\text{m}^3/\text{cm}^3$ and $6 \pm 8 \mu\text{m}^3/\text{cm}^3$ for fine and total volume concentrations, respectively. In contrast,
285 better correlation is observed for coarse mode volume concentrations (slope equals to 1) with
a lower mean difference ($2 \pm 6 \mu\text{m}^3/\text{cm}^3$). In terms of absolute concentrations, 65% (91%),
70% (88%) and 45% (71%) of the differences are observed within $\pm 5 \mu\text{m}^3/\text{cm}^3$ ($\pm 10 \mu\text{m}^3/\text{cm}^3$)
for fine, coarse and total volume concentrations, respectively. These results are similar to those
found in previous GRASP assessments by Benavent-Oltra et al. (2017) and Tsekeri et al.
290 (2017). Those authors also showed an overestimation of VC_F compared with in-situ data, while
for VC_C similar GRASP retrievals to in-situ data was found for cases with coarse particles
predominate. The observed overestimation is lower than the obtained by Román et al. (2018)
using GRASP with ceilometer data, and by Benavent-Oltra et al. (2019) using GRASP with
lidar emission signals at 355, 532 and 1064 nm. Titos et al. (2019) found that the agreement



295 between GRASP retrievals (from ceilometer measurements) and in-situ data improved when
the contribution of fine particles was negligible.

[Figure 2]

Figure 3 shows σ_{sca} and σ_{abs} obtained by GRASP at ~ 2.5 km height versus those
obtained by in-situ measurements at SNS. The comparison has been performed interpolating
300 the GRASP values at 355, 532 and 1064 nm to the wavelengths of the nephelometer (450, 550
and 700 nm) and the aethalometer (370, 520 and 880 nm) by the Ångström exponent law. For
the σ_{sca} , we can observe that generally the agreements between GRASP and in-situ data are
similar at the three wavelengths ($R \sim 0.95$). The slopes of the linear fits are equal to 1 with an
intercept lower than 10 Mm^{-1} that decreases for larger wavelengths. Globally, GRASP
305 overestimates in-situ data at SNS with a mean difference (\pm standard deviation) of $11 \pm 17 \text{ Mm}^{-1}$,
 $6 \pm 14 \text{ Mm}^{-1}$ and $4 \pm 11 \text{ Mm}^{-1}$ at 450, 550 and 700 nm, respectively. On the other hand, for
 σ_{abs} , GRASP shows good correlation with the in-situ data with correlation coefficients around
0.85. In general, GRASP overestimates the in-situ data at SNS as shown the slopes (~ 1.2) and
intercepts (from 0.5 to 1.5 Mm^{-1}) of the regressions. The mean differences (\pm standard
310 deviation) of σ_{abs} $2 \pm 6 \text{ Mm}^{-1}$, $1 \pm 3 \text{ Mm}^{-1}$ and $0.8 \pm 1.7 \text{ Mm}^{-1}$ at 370, 520 and 880 nm,
respectively. Furthermore, the differences between GRASP and in-situ measurements are less
than $\pm 2.5 \text{ Mm}^{-1}$ for 61%, 81% and 90% of the data at 370, 520 and 880 nm, respectively. The
results from Figure 3 for the validation of σ_{sca} are similar to previous validations of GRASP
retrievals with in-situ data from high mountain sites (e.g. Titos et al., 2019; Benavent-Oltra et
315 al., 2019). However, it should be noted that the results presented here are the first direct
validation of retrieved σ_{abs} .

Finally, the comparison between GRASP retrievals and in-situ data for extinction
coefficient showed in Figure 4a evidence better agreement. The GRASP retrievals and in-situ
data show good agreement (slope equals to 1) and are highly correlated ($R = 0.9$). Figure 4b
320 shows the frequency histogram of the differences in extinction coefficient ($\Delta\alpha$) between
GRASP and in-situ, showing a skewed histogram to positive differences that implies slightly
overestimation by GRASP (75% of these differences within $\pm 15 \text{ Mm}^{-1}$). These overestimations
can be associated with the differences in scattering coefficient.

[Figure 3]

325 **[Figure 4]**



4.1.2. Aircraft profiles

A total of 6 flights were carried out on 15th, 17th and 18th June 2016 during SLOPE I and 21st, 23rd and 24th June 2017 during SLOPE II. During the SLOPE I flights, the aerosol conditions were characterized by AOD values at 440 nm (AOD₄₄₀) lower than 0.1 and Ångström exponent (AE), computed with AOD at 440 and 870 nm (AE_{440–870}), between 0.6 and 1.3. On the other hand, during the week of flights in the SLOPE II there was a dust intrusion from Sahara Desert with higher AOD₄₄₀ values (ranging from 0.13 to 0.36 on 23rd and 24th June 2017, respectively) and low AE_{440–870} values between 0.3 and 0.8. Figure 5 shows the vertical profiles of scattering and absorption coefficients retrieved by GRASP code and measured by the on-board instrumentation. This figure also includes the mean value measured at SNS station during the flights. For the sake of comparison, the GRASP values at 355, 532 and 1064 nm has been interpolated to the nephelometer and aethalometer wavelengths using the Ångström exponent law.

[Figure 5]

For σ_{sca} , both GRASP and airborne measurements follow the same pattern where GRASP overestimates the airborne data with a mean absolute difference of $14 \pm 10 \text{ Mm}^{-1}$. During SLOPE I, these mean absolute differences are lower than 8 Mm^{-1} and there is a good agreement between GRASP and SNS measurements (differences $<4 \text{ Mm}^{-1}$). However, during SLOPE II, the differences between GRASP and in situ measurements (both airborne and SNS) are larger, reaching values of 30 Mm^{-1} . In the case of σ_{abs} , GRASP and airborne profiles show large differences during SLOPE I with mean absolute differences between 0.5 and 3 Mm^{-1} reaching differences around 6 Mm^{-1} on 18th June 2016. On the other hand, the absorption coefficients retrieved by GRASP show good agreement within situ measurements (both airborne and SNS) with a mean absolute difference of $0.7 \pm 0.4 \text{ Mm}^{-1}$ during SLOPE II. In general, the differences between GRASP and in situ measurements are close to the detection limit for the aethalometer on-board the airplane and SNS. The differences obtained both for σ_{sca} and σ_{abs} can be explained due to the low AOD₄₄₀ (below 0.40) that represents a challenge for the retrieval of the aerosol properties both for AERONET (Dubovik and King, 2000; Dubovik et al., 2000) and inversion algorithms as GRASP (Lopatin et al., 2013). However, the very good agreement in absorption coefficient during SLOPE II indicates the good capability of GRASP to retrieve vertical profiles of absorption to AOD₄₄₀ higher 0.1.



4.2. Aerosol properties during SLOPE I and II

4.2.1. Column-integrated

Figure 6 shows the temporal evolutions of AOD₄₄₀ and AE_{440–870} daily mean values retrieved
360 by GRASP code at UGR during SLOPE I and II campaigns. Daily averaged values of AOD₄₄₀
retrieved by GRASP code ranges from 0.06 to 1.0, with a mean (\pm standard deviation) value of
0.22 \pm 0.18, while AE_{440–870} varies from 0.11 to 1.6 with a mean value of 0.8 \pm 0.4. The large
variability of AODs and Ångström exponents observed in Figure 6 are typical for this season
in the study area (e.g. Perez-Ramirez et al., 2012). Large AODs and low AE values as those
365 observed on 20th July 2016 are related to Saharan dust outbreaks (e.g. Román et al., 2018;
Benavent-Oltra et al., 2019), while large AODs and AE values as those observed on 26th July
2017 are related to a biomass burning transport (from Portugal in this case) (Turco et al., 2019).

[Figure 6]

Figure 7 shows the Box-Wisher diagrams of retrieved aerosol columnar-integrated
370 properties such as SSA, LR and aerosol absorption optical depth (AAOD) at 355, 440, 532,
675, 870, 1020 and 1064 nm retrieved by GRASP code during the study period. For aerosol
intensive properties, the SSA values are typical for Saharan dust outbreaks at the study region
(e.g. Valenzuela et al., 2012), ranging from 0.88 \pm 0.05 at 355 nm to 0.90 \pm 0.06 at 1064 nm,
respectively. These relatively large values of SSA for all wavelengths indicate important
375 fraction of non-absorbing aerosol particles. The LR values show large wavelength-variability,
with mean values ranged from 80 \pm 30 sr at 355 nm to 35 \pm 16 sr at 1064 nm, being typical for
Saharan desert dust (Shin et al., 2018). For aerosol extensive properties, the highest AAODs
($>$ 0.10) correspond both to dust and biomass-burning events, with an absorption Ångström
exponent (AAE; computed in the spectral range 355–1064 nm) higher than 1.5 for desert dust
380 event and around 1.0 for biomass burning event. The variability in AAE can be explained by
the differences in particles chemical compositions, but in frame of the current capabilities in
GRASP retrievals we could not advance with such analyses. Nevertheless, GRASP has
revealed the large contribution of aerosol absorption in total aerosol optical depth during
SLOPE I and II field campaigns even for cases with relatively low AODs.

385

[Figure 7]

The large standard deviations and percentiles observed in Figure 7 for all aerosol optical
properties agree with the variability of aerosol types deduced from Figure 6. The aerosol
variability can be caused by the fact that the different air-masses reach the south-east of Spain.



Usually, the air-masses in the study region come from the Atlantic bringing clean air, from
390 North of Africa transporting mineral dust, or from the Mediterranean transporting
anthropogenic particles (e.g. Perez-Ramirez et al., 2016). Another frequent source of aerosol
particles are the biomass burning events near to the study region (Alados-Arboledas et al.,
2011; Ortiz-Amezcuca et al., 2017; Sicard et al., 2019). According to the warning system of
natural aerosol episodes of MITECO (Spanish Ministry for Ecological Transition and
395 Demographic Challenge, <https://www.miteco.gob.es/es/calidad-y-evaluacion-ambiental/temas/>, last access: 1 June 2020), around the 66% and 10% of the evaluated days
with GRASP retrievals there were associated to North African intrusions and biomass burning
events in the south-eastern of Spain, respectively.

4.2.2. Vertically-resolved

400 Figure 8 shows a statistical overview of the aerosol optical and microphysical properties
profiles retrieved by GRASP: volume concentration, differentiating between fine and coarse
mode, and for the aerosol optical properties the extinction, scattering and absorption
coefficients plus SSA and LR, all at the reference wavelength of 532 nm. Additionally, we
include the AAE and SAE computed between 355 and 1064 nm. The solid black lines represent
405 the medians and red dashed line the means. The shadowed area is the interquartile range and
the black dashed lines represent 10th and 90th percentiles.

For aerosol microphysical properties (Figures 8a, b) we observe approximately a linear
decay with altitude until they reach approximately zero at 4-5 km a.s.l.. These decays do not
reveal any decoupled layer with altitude. The largest values are at the lowest altitudes (with
410 average $\sim 10 \mu\text{m}^3/\text{cm}^3$). The VC_F profile shows lower variability (smaller interquartile range)
than VC_C profile. The highest variability of coarse particles profile, being the 90th percentile
with values between 40 and $60 \mu\text{m}^3/\text{cm}^3$, is mainly caused by the intrusion of desert dust
particles during SLOPE I and II campaigns.

[Figure 8]

415 The extinction, scattering and absorption coefficients profiles at 532 nm (Fig 8 c, d, e)
show similar behaviour than VC profiles. These pattern of extinction coefficient profiles for
long-term statistical analyses have been observed in Europe for previous studies using Raman
lidar data (e.g. Amiridis et al., 2005; Navas-Guzmán et al., 2013). The largest values for the
particle extinction, scattering and absorption coefficients are observed at the lowest altitudes
420 (40, 35 and 4 Mm^{-1} for α , σ_{sca} and σ_{abs} , respectively). Moreover, a clear exponential decrease



is observed for the mean σ_{sca} and σ_{abs} coefficients. This behaviour was also observed in other statistical lidar studies (e.g. Titos et al., 2019). The SSA profile at 532 nm decreases with values from 0.92 at lowest altitude to 0.86 at highest altitude, and with interquartile range ~ 0.025 which is close to the uncertainties claimed for SSA retrievals using remote sensing techniques (e.g. Pérez-Ramírez et al., 2019). The combination of σ_{abs} and SSA reveal that for the entire profile approximately 10% of total extinction corresponds to absorption. Thus, GRASP retrieval combining several remote sensing instruments presents a step forward to aerosol characterization because permits characterizing aerosol absorption with vertical resolution and for lower aerosol loads than classical AERONET inversion.

The profiles of intensive properties (LR, AAE and SAE) can provide information about predominance of different aerosol particles types. For LR at 532 nm (Figure 8g), a constant mean profile is observed with mean value of ~ 52 sr. LR at a given wavelength depends mainly both on chemical composition and particle shapes, which explains the variability in the retrieved values for the variable aerosol types, registered during SLOPE I and II, with a strong contribution of mineral dust (Müller et al., 2007). The LR values obtained are very similar to observed in other studies (e.g. Guerrero-Rascado et al., 2009; Navas-Guzmán et al., 2013a). For SAE (Figure 8h), which is more related to the predominant particle size, the highest value is found at the lowest altitude, suggesting larger predominance of fine particles closer to the surface. This pattern agrees with the assumption of higher anthropogenic aerosol loads at these levels are dominated by fine mode particles, while at altitudes above the atmospheric boundary layer top is observed typically transported mineral dust (coarse particles) with low mixture of anthropogenic pollution. Finally, AAE (Figure 8i), that is related with the chemical composition of the absorbing aerosol, follows a constant pattern with altitude with mean value of ~ 1.45 with a 10th and 90th percentiles equal to 1 and 2, respectively. These are the values typically found for Saharan mineral dust particles transport and their mixture with anthropogenic pollutions (Russell et al., 2010).

4.2.3. Special Events

During the SLOPE I and II campaigns two extreme events with $AOD_{440} \sim 1.0$ were registered. The first one was a Saharan mineral dust outbreak (DD) in July 2016, and the second one was a biomass burning transport event (BB) in July 2017 with fires origin in Portugal. Figure 9 and 10 show the profiles of aerosol optical and microphysical properties for the DD and BB event, respectively. It is also included in these figures the time when retrievals were obtained, the AOD at each moment and the SNS measurements at available periods.



[Figure 9]

455 Figure 9 and 10 show that for the first day of each event (20th July 2016 and 26th July
2017) decoupled aerosol layers were observed at ~ 4 km a.s.l., approximately. Such decoupled
layers went gradually downward until they reached the altitude of ~ 2-3 km a.s.l. on the
morning of the second day of the event, on 21st July 2016 and 27th July 2017, respectively. This
phenomenon is known as entrainment event and it has been observed previously in our region
460 (Bravo-Aranda et al., 2015). These figures suggest that these entrainments affect both to
intensive and extensive aerosol properties.

The analyses of microphysical properties profiles show important differences in volume
concentration between these two extreme events. For DD event, coarse particles predominate
with VC_C between 200 and 300 $\mu\text{m}^3/\text{cm}^3$ on the aerosol layer, while for the BB event, the VC_C
465 is very low ($\sim 10 \mu\text{m}^3/\text{cm}^3$) and fine particles predominate with maximum values between 60
and 105 $\mu\text{m}^3/\text{cm}^3$. In general, GRASP VC_F overestimate SNS measurements with differences
below 10 $\mu\text{m}^3/\text{cm}^3$, whereas GRASP VC_C is similar to SNS measurements for values around
55 $\mu\text{m}^3/\text{cm}^3$ as shown in the Section 4.1.1.. However, for higher values of VC_C , GRASP
overestimates the SNS data with differences between 10 and 20 $\mu\text{m}^3/\text{cm}^3$ as shown Benavent et
470 al. (2019).

For intensive optical properties, the σ_{sca} profiles at 532 nm show similar values
between both events, with values between 200 and 400 Mm^{-1} . These similarities in σ_{sca} are
explained because total scattering is directly associated with the total aerosol load, which is
very similar between both extreme events. However, for σ_{abs} there are significant differences
475 between both events, being observed larger values during the BB event probably because the
presence of organic and black carbon particles. Nevertheless, we remark that σ_{abs} is not
negligible as expected for mineral dust particles (e.g. Valenzuela et al., 2012). These findings
are support from SSA profiles that shows lower SSA values for biomass burning (mean values
 ~ 0.83), and higher for dust events (mean values around 0.93).

480 Finally, Figures 9 and 10 also show the profiles obtained for intensive properties such
as SAE and AAE, computed from GRASP retrievals (spectral range 355-1064 nm). The
analyses of these variables can provide an indication of aerosol types. On 20th and 21st July
2016, the SAE values lower than 0.5 corroborate the predominance of coarse particles for
mineral dust particles (Bergstrom et al., 2007), and the AAE values, ranging from 1.5 to 2.1,
485 suggest a mixture of mineral dust and absorbing particles of anthropogenic origin (e.g. Giles et



al., 2011; Valenzuela et al., 2015). During the BB event, the SAE values are around 2, indicating a scattering dominated by submicron particles, and the AAE values between 1.1 and 1.45 suggest the presence of carbonaceous particles (Giles et al., 2012). Nevertheless, further advancement in the interpretation of aerosol chemical composition is challenging now, while
490 new development aiming on characterization of aerosol compositions are being included into GRASP (Li et al., 2019, 2020) and to be explored in the future.

5. Conclusions

In this study, we presented an overview of aerosol optical and microphysical properties retrieved with GRASP code during SLOPE I and II field campaigns. The measurements from
495 lidar and sun-sky photometer performed on May, June and July 2016 and 2017 were used as input data in GRASP to retrieve these aerosol properties.

The in-situ measurements performed at Sierra Nevada Station during SLOPE I and II campaigns, and the airborne measurement gathered during special periods on both campaigns allowed the assessment of aerosol properties retrieved by GRASP code at 2.5 km a.s.l. and for the whole profile, respectively. The volume concentration comparison shows better agreement
500 for coarse mode ($R > 0.8$) than for fine mode due to the few cases (15%) with predominating fine particles. For the scattering and absorption coefficients, the differences between GRASP data at 2.5 km a.s.l. and in-situ measurements are lowest for longest wavelengths, with differences of $11 \pm 17 \text{ Mm}^{-1}$ at 450 nm and $2 \pm 6 \text{ Mm}^{-1}$ at 370 nm for σ_{sca} and σ_{abs} ,
505 respectively. The agreement between GRASP and in-situ measurements at SNS is solid for both for scattering and absorption coefficients. In general, GRASP somewhat overestimates the in-situ data at 2.5 km a.s.l.. These differences (14 ± 10 and $1.2 \pm 1.2 \text{ Mm}^{-1}$ σ_{sca} and σ_{abs} , respectively) are also observed in the whole profile when comparing GRASP retrievals and the airborne measurements performed on 15th, 17th and 18th June 2016 and 21st, 23rd and 24th June
510 2017.

The statistical analysis of SLOPE I and II campaigns show the values of aerosol optical depth ($\text{AOD}_{440} = 0.22 \pm 0.18$) and Ångström exponent ($\text{AE}_{440-870} = 0.8 \pm 0.4$) that are typical of those months in Granada. The large variety of aerosol properties values denotes a large variability of aerosol loads and types with a desert mineral dust predominance associated with
515 North African intrusions in the south-eastern of Spain. The statistical overview of the volume concentration profiles shows a decay of the properties with the altitude, reaching approximately zero at 4-5 km a.s.l.. The coarse mode shows the highest variability being the 90th percentile



with values between 40 and 60 $\mu\text{m}^3/\text{cm}^3$. The largest value for the absorption coefficient is observed at the lowest altitudes (4 Mm^{-1}). Finally, two extreme events ($\text{AOD}_{440} > 1.0$) were studied: Saharan desert dust intrusion and biomass burning from Portugal fires in July 2016 and 2017, respectively. The study of these events shows the high capabilities of GRASP to retrieve volume concentration profiles in both fine and coarse mode and potentially interesting capability of the algorithm to derive the profiles of the single scattering albedo and absorption coefficients for different types and sizes of atmospheric aerosols.

525

Data availability. The GRASP inversion algorithm software used in this work is free and publicly available at <http://www.grasp-open.com> (last access: 1 April 2020). Lidar and in-situ data are available from the authors upon request. Sun–sky photometer data are accessible on the AERONET website (<http://aeronet.gsfc.nasa.gov/>, last access: 1 April 2020).

530

Author contributions. The conceptualization was done by JABO and LAA. JABO performed the GRASP retrievals, analysed the data and wrote the manuscript. RR helped to perform GRASP retrievals. JACV and HL operated and processed the in-situ measurement at Sierra Nevada Station. GT, NP and AA performed the installation of the instrumentation on-board the aircraft and operated the instruments during the flights. AC processed the airborne in-situ data. The lidar data acquisition was performed by JABO, GdAM, JLGR, POA, RR, and AEBV. MH and OD provided feedback on the GRASP algorithm. The formal analysis, investigation, writing of the original draft, preparation, review of the writing and editing were performed by JABO, JACV, RR, DPR, HL and MJGM. The project administration, funding acquisition and design of SLOPE I and II campaigns were done by FJOR and LAA. Coordination of the campaign has been responsibility of LAA. All authors provided comments on the manuscript and helped with paper correction.

540

Competing interests. The authors declare that they have no conflict of interest.

545

Acknowledgements. Jose Antonio Benavent-Oltra is funded by the University of Granada through “Plan Propio. Programa 7, Convocatoria 2019”. Roberto Román is funded by MINECO under the postdoctoral programme Juan de la Cierva-Incorporación (IJCI2016-30007). Juan Andrés Casquero-Vera is funded by MINECO under the predoctoral programme



550 FPI (BES-2017-080015). Oleg Dubovik was supported by the Labex CaPPA project, which is funded by the French National Research Agency under contract “ANR-11-LABX0005-01”. The authors thankfully acknowledge the FEDER programme for the instrumentation used in this work, the University of Granada, which supported this study through the excellence units programme, and the Sierra Nevada National Park. We also thank Dr. Grisa Monick who
555 provided the Aethalometer AVIO AE-33 installed on the aircraft. Thanks to AERONET and ACTRIS/AERONET-Europe for the scientific and technical support. Finally, the authors would like to acknowledge the use of the GRASP inversion algorithm software (<http://www.grasp-open.com>, last access: 1 April 2020) in this work.

Financial support. This research has been supported by the Spanish Ministry of Economy and
560 Competitiveness (projects CMT2015-66742-R, CGL2016-81092- R, CGL2017-85344-R, RTI2018-097864-B-I00 and CGL2017- 90884-REDT), by by the Andalusia Regional Government through project P18-RT-3820, and by the Marie Skłodowska-Curie Research Innovation and Staff Exchange (RISE) GRASP-ACE (grant no. 778349) project. The authors thankfully acknowledge the University of Granada that supported this study through the
565 Excellence Units Program

References

- Alados-Arboledas, L., Muller, D., Guerrero-Rascado, J. L., Navas-Guzman, F., Pérez-Ramírez, D., and Olmo, F. J.: Optical and microphysical properties of fresh biomass burning aerosol retrieved by Raman lidar, and star-
570 and sun-photometry, *Geophys. Res. Lett.*, 38, L01807, <https://doi.org/10.1029/2010GL045999>, 2011.
- Amiridis, V., Balis, D. S., Kazadzis, S., Bais, A., Giannakaki, E., Papayannis, A., and Zerefos, C.: Four-year aerosol observations with a Raman lidar at Thessaloniki, Greece, in the framework of European Aerosol Research Lidar Network (EARLINET), *J. Geophys. Res.*, 110, D21203, <https://doi.org/10.1029/2005JD006190>, 2005.
- 575 Anderson, T.L., and Ogren, J. A.: Determining aerosol radiative properties using the TSI 3563 integrating nephelometer, *Aerosol Sci. Technol.*, 29, 57–69, 1998.
- Ansmann, A., Riebesell, M., Wandinger, U., Weitkamp, C., Voss, E., Lahmann, W., and Michaelis, W.: Combined Raman elastic backscatter LIDAR vertical profiling of moisture, aerosol extinction, backscatter and LIDAR ratio, *Appl. Phys. B*, 55, 18–28, 1992.
- 580 Barreto, Á., Cuevas, E., Granados-Muñoz, M. J., Alados-Arboledas, L., Romero, P. M., Gröbner, J., Kouremeti, N., Almansa, A. F., Stone, T., Toledano, C., Román, R., Sorokin, M., Holben, B., Canini, M., and Yela, M.: The new sun-skyline Cimel CE318-T multiband photometer – a comprehensive performance evaluation, *Atmos. Meas. Tech.*, 9, 631–654, <https://doi.org/10.5194/amt-9-631-2016>, 2016.
- 585 Barreto, Á., Román, R., Cuevas, E., Pérez-Ramírez, D., J. Berjón, A., Kouremeti, N., Kazadzis, S., Gröbner, J., Mazzola, M., Toledano, C., Benavent-Oltra, J. A., Doppler, L., Juryšek, J., Almansa, A. F., Victori, S., Maupin, F., Guirado-Fuentes, C., González, R., Vitale, V., Goloub, P., Blarel, L., Alados-Arboledas, L., Woolliams, E., Greenwell, C., Taylor, S., Antuña, J. C., and Yela, M.: Evaluation of night-time aerosols measurements and lunar irradiance models in the frame of the first multi-instrument nocturnal intercomparison campaign, *Atmos. Environ.*, 202, 190-211, <https://doi.org/10.1016/j.atmosenv.2019.01.006>, 2019.
- 590 Bedoya-Velásquez, A. E., Navas-Guzmán, F., Granados-Muñoz, M. J., Titos, G., Román, R., Casquero-Vera, J. A., Ortiz-Amezcuca, P., Benavent-Oltra, J. A., de Arruda Moreira, G., Montilla-Rosero, E., Hoyos, C. D., Artiñano, B., Coz, E., Olmo-Reyes, F. J., Alados-Arboledas, L., and Guerrero-Rascado, J. L.: Hygroscopic



- growth study in the framework of EARLINET during the SLOPE I campaign: synergy of remote sensing and in situ instrumentation, *Atmos. Chem. Phys.*, 18, 7001-7017, <https://doi.org/10.5194/acp-18-7001-2018>, 2018.
- 595 Bedoya-Velásquez, A.E., Navas-Guzmán, F., de Arruda Moreira, G., Román, R., Cazorla, A., Ortiz-Amezcuca, P., Benavent-Oltra, J.A., Alados-Arboledas, L., Olmo-Reyes, F.J., Foyo-Moreno, I., Montilla-Rosero, E., Hoyos, C.D., Guerrero-Rascado, J.L. Seasonal analysis of the atmosphere during five years by using microwave radiometry over a mid-latitude site. *Atmospheric Research*, 218, pp. 78-89, <https://doi.org/10.1016/j.atmosres.2018.11.014>, 2019.
- 600 Benavent-Oltra, J. A., R. Román, M. J. Granados-Muñoz, D. Pérez-Ramírez, P. Ortiz-Amezcuca, C. Denjean, A. Lopatin, H. Lyamani, B. Torres, J. L. Guerrero-Rascado, D. Fuertes, O. Dubovik, A. Chaikovsky, F. J. Olmo, M. Mallet, and L. Alados-Arboledas: Comparative assessment of GRASP algorithm for a dust event over Granada (Spain) during ChArMEX-ADRIMED 2013 campaign, *Atmos. Meas. Tech.*, 10, 4439-4457, <https://doi.org/10.5194/amt-10-4439-2017>, 2017.
- 605 Benavent-Oltra, J. A., Román, R., Casquero-Vera, J. A., Pérez-Ramírez, D., Lyamani, H., Ortiz-Amezcuca, P., Bedoya-Velásquez, A. E., de Arruda Moreira, G., Barreto, Á., Lopatin, A., Fuertes, D., Herrera, M., Torres, B., Dubovik, O., Guerrero-Rascado, J. L., Goloub, P., Olmo-Reyes, F. J., and Alados-Arboledas, L.: Different strategies to retrieve aerosol properties at night-time with the GRASP algorithm, *Atmos. Chem. Phys.*, 19, 14149-14171, <https://doi.org/10.5194/acp-19-14149-2019>, 2019.
- 610 Bergstrom, R.W., Pilewskie, P., Russell, P. B., Redemann, J., Bond, T. C., Quinn, P. K., and Sierau, B.: Spectral absorption properties of atmospheric aerosols, *Atmos. Chem. Phys.*, 7, 5937-5943, <https://doi.org/10.5194/acp-7-5937-2007>, 2007.
- Böckmann, C.: Hybrid regularization method for the ill-posed inversion of multiwavelength lidar data to determine aerosol size distributions, *Appl. Optics*, 40, 1329-1342, 2001.
- 615 Bravo-Aranda, J. A., Titos, G., Granados-Muñoz, M. J., Guerrero-Rascado, J. L., Navas-Guzmán, F., Valenzuela, A., Lyamani, H., Olmo, F. J., Andrey, J., and Alados-Arboledas, L.: Study of mineral dust entrainment in the planetary boundary layer by lidar depolarisation technique, *Tellus B*, 67, 26180, doi:10.3402/tellusb.v67.26180, 2015.
- 620 Cariñanos, P., Foyo-Moreno, I., Alados, I., Guerrero-Rascado, J.L., Ruiz-Peñuela, S., Titos, G., Cazorla, A., Alados-Arboledas, L. and Díaz de la Guardia, C. Bioaerosols in urban environments: Trends and interactions with pollutants and meteorological variables based on quasi-climatological series, *Journal of Environmental Management*, 282, 111963, <https://doi.org/10.1016/j.jenvman.2021.111963>, 2021.
- Casquero-Vera, J. A., Lyamani, H., Dada, L., Hakala, S., Paasonen, P., Román, R., Fraile, R., Petäjä, T., Olmo-Reyes, F. J., and Alados-Arboledas, L.: New particle formation at urban and high-altitude remote sites in the south-eastern Iberian Peninsula, *Atmos. Chem. Phys. Discuss.*, <https://doi.org/10.5194/acp-2020-394>, in review, 2020.
- 625 Casquero-Vera J.A., Lyamani H., Titos G., Minguillón M.C., Dada L., Alastuey A., Querol X., Petäjä T., Olmo F.J., Alados-Arboledas L.: Quantifying traffic, biomass burning and secondary source contributions to atmospheric particle number concentrations at urban and suburban sites, *Science of the Total Environment*, 2021.
- 630 Caumont, O., Cimini, D., Löhnert, U., Alados-Arboledas, L., Bleisch, R., Buffa, F., Ferrario, M. E., Haeefe, A., Huet, T., Madonna, F., and Pace, G.: Assimilation of humidity and temperature observations retrieved from ground-based microwave radiometers into a convective-scale NWP model, *Q. J. Roy. Meteorol. Soc.*, 142, 2692-2704, <https://doi.org/10.1002/qj.2860>, 2016.
- 635 Chaikovsky, A., Dubovik, O., Goloub, P., Balashevich, N., Lopatsin, A., Karol, Y., Denisov, S. and Lapyonok, T.: Software package for the retrieval of aerosol microphysical properties in the vertical column using combined lidar/photometer data (test version), Technical Report, Minsk, Belarus, Institute of Physics, National Academy of Sciences of Belarus, 2008.
- 640 Chaikovsky, A., Dubovik, O., Holben, B., Bril, A., Goloub, P., Tanré, D., Pappalardo, G., Wandinger, U., Chaikovskaya, L., Denisov, S., Grudo, J., Lopatin, A., Karol, Y., Lapyonok, T., Amiridis, V., Ansmann, A., Apituley, A., Alados-Arboledas, L., Biniotoglou, I., Boselli, A., D'Amico, G., Freudenthaler, V., Giles, D., Granados-Muñoz, M. J., Kokkalis, P., Nicolae, D., Oshchepkov, S., Papayannis, A., Perrone, M. R., Pietruczuk, A., Rocadenbosch, F., Sicard, M., Slutsker, I., Talianu, C., De Tomasi, F., Tsekeri, A., Wagner, J., and Wang, X.: Lidar-Radiometer Inversion Code (LIRIC) for the retrieval of vertical aerosol properties from combined lidar/radiometer data: development and distribution in EARLINET, *Atmos. Meas. Tech.*, 9, 1181-1205, <https://doi.org/10.5194/amt-9-1181-2016>, 2016.
- 645 Chen, C., Dubovik, O., Henze, D. K., Lapyonok, T., Chin, M., Ducos, F., Litvinov, P., Huang, X., and Li, L.: Retrieval of desert dust and carbonaceous aerosol emissions over Africa from POLDER/PARASOL products



- 650 generated by the GRASP algorithm, *Atmos. Chem. Phys.*, 18, 12551–12580. <https://doi.org/10.5194/acp-18-12551-2018>, 2018.
- Chen, C., Dubovik, O., Henze, D. K., Chin, M., Lapyonok, T., Schuster, G. L., Ducos, F., Fuertes, D., Litvinov, P., Li, L., Lopatin, A., Hu, Q., and Torres, B.: Constraining global aerosol emissions using POLDER/PARASOL satellite remote sensing observations, *Atmos. Chem. Phys.*, 19, 14585–14606, <https://doi.org/10.5194/acp-19-14585-2019>, 2019.
- 655 de Arruda Moreira, G., Guerrero-Rascado, J. L., Bravo-Aranda, J. A., Benavent-Oltra, J. A., Ortiz-Amezcuca, P., Román, R., Bedoya-Velásquez, A. E., Landulfo, E., and Alados-Arboledas, L.: Study of the planetary boundary layer by microwave radiometer, elastic lidar and Doppler lidar estimations in Southern Iberian Peninsula, *Atmos. Res.*, 213, 185–195, <https://doi.org/10.1016/j.atmosres.2018.06.007>, 2018.
- 660 de Arruda Moreira, G., Guerrero-Rascado, J. L., Benavent-Oltra, J. A., Ortiz-Amezcuca, P., Román, R., E. Bedoya-Velásquez, A., Bravo-Aranda, J. A., Olmo Reyes, F. J., Landulfo, E., and Alados-Arboledas, L.: Analyzing the turbulent planetary boundary layer by remote sensing systems: the Doppler wind lidar, aerosol elastic lidar and microwave radiometer, *Atmos. Chem. Phys.*, 19, 1263–1280, <https://doi.org/10.5194/acp-19-1263-2019>, 2019.
- 665 del Águila, A., Sorribas, M., Lyamani, H., Titos, G., Olmo, F.J., Arruda-Moreira, G., Yela, M., Alados-Arboledas, L. Sources and physicochemical characteristics of submicron aerosols during three intensive campaigns in Granada (Spain), <https://doi.org/10.1016/j.atmosres.2018.06.004>, *Atmospheric Research*, 213, pp. 398–410, 2018.
- Dubovik, O. and M. D. King, “A flexible inversion algorithm for retrieval of aerosol optical properties from Sun and sky radiance measurements”, *J. Geophys. Res.*, 105, 20,673–20,696, 2000.
- 670 Dubovik, O., Smirnov, A., Holben, B.N., King, M.D., Kaufman, Y., Eck, T.F., Slutsker, I.: Accuracy assessments of aerosol optical properties retrieved from AerosolRobotic Network (AERONET) Sun and sky radiance measurements. *J. Geophys. Res.* 105, 9791–9806, 2000.
- Dubovik, O., M. Herman, A. Holdak, T. Lapyonok, D. Tanré, J. L. Deuzé, F. Ducos, A. Sinyuk, and A. Lopatin, “Statistically optimized inversion algorithm for enhanced retrieval of aerosol properties from spectral multi-angle polarimetric satellite observations”, *Atmos. Meas. Tech.*, 4, 975–1018, 2011.
- 675 Dubovik, O., Lapyonok, T., Litvinov, P., Herman, M., Fuertes, D., Ducos, F., Lopatin, A., Chaikovskiy, A., Torres, B., Derimian, Y., Huang, X., Lopatin, A., Chaikovskiy, A., Aspetsberger, M., and Federspiel, C.: Grasp: a versatile algorithm for characterizing the atmosphere. *SPIE Newsroom*, 25, 2014.
- 680 Dubovik, O., Li, Z., Mishchenko, M. I., Tanré, D., Karol, Y., Bojkov, B., Cairns, B., Diner, D. J., Espinosa, W. R., Goloub, P., Gu, X., Hasekamp, O., Hong, J., Hou, W., Knobelspiess, K. D., Landgraf, J., Li, L., Litvinov, P., Liu, Y., Lopatin, A., Marbach, T., Maring, H., Martins, V., Meijer, Y., Milinevsky, G., Mukai, S., Parol, F., Qiao, Y., Remer, L., Rietjens, J., Sano, I., Stammes, P., Stammes, S., Sun, X., Tabary, P., Travis, L. D., Waquet, F., Xu, F., Yan, C., and Yin, D.: Polarimetric remote sensing of atmospheric aerosols: Instruments, methodologies, results, and perspectives, *J. Quant. Spectrosc. Ra.*, 224, 474–511, <https://doi.org/10.1016/j.jqsrt.2018.11.024>, 2019.
- 685 Drinovec, L., Močnik, G., Zotter, P., Prévôt, A. S. H., Ruckstuhl, C., Coz, E., Rupakheti, M., Sciare, J., Müller, T., Wiedensohler, A., and Hansen, A. D. A.: The “dual-spot” Aethalometer: an improved measurement of aerosol black carbon with real-time loading compensation, *Atmos. Meas. Tech.*, 8, 1965–1979, <https://doi.org/10.5194/amt-8-1965-2015>, 2015.
- 690 Espinosa, W. R., Remer, L. A., Dubovik, O., Ziemba, L., Beyersdorf, A., Orozco, D., Schuster, G., Lapyonok, T., Fuertes, D., and Martins, J. V.: Retrievals of aerosol optical and microphysical properties from Imaging Polar Nephelometer scattering measurements, *Atmos. Meas. Tech.*, 10, 811–824, <https://doi.org/10.5194/amt-10-811-2017>, 2017.
- 695 Fernald, F. G., Herman, B. M., and Reagan, J. A.: Determination of aerosol height distributions by lidar, *J. Appl. Meteorol.*, 11, 482–489, 1972.
- Fernald, F. G.: Analysis of atmospheric lidar observations- Some comments, *App. Optics*, 23, 652–653, 1984.
- Giles, D. M., Holben, B. N., Tripathi, S. N., Eck, T. F., Newcomb, W. W., Slutsker, I., Dickerson, R. R., Thompson, A. M., Mattoo, S., Wang, S., Singh, R. P., Sinyuk, A., and Schafer, J. S.: Aerosol properties over the Indo-Gangetic Plain: A mesoscale perspective from the TIGERZ experiment, *J. Geophys. Res.-Atmos.*, 116, D18203, <https://doi.org/10.1029/2011JD015809>, 2011.
- 700 Giles, D. M., Holben, B. N., Eck, T. F., Sinyuk, A., Smirnov, A., Slutsker, I., Dickerson, R. R., Thompson, A. M., and Schafer, J. S.: An analysis of AERONET aerosol absorption properties and classifications representative of aerosol source regions, *J. Geophys. Res.-Atmos.*, 117, 127–135, <https://doi.org/10.1029/2012JD018127>, 2012.



- 705 Giles, D. M., Sinyuk, A., Sorokin, M. G., Schafer, J. S., Smirnov, A., Slutsker, I., Eck, T. F., Holben, B. N., Lewis, J. R., Campbell, J. R., Welton, E. J., Korokin, S. V., and Lyapustin, A. I.: Advancements in the Aerosol Robotic Network (AERONET) Version 3 database – automated near-real-time quality control algorithm with improved cloud screening for Sun photometer aerosol optical depth (AOD) measurements, *Atmos. Meas. Tech.*, 12, 169–209, <https://doi.org/10.5194/amt-12-169-2019>, 2019.
- 710 Granados-Muñoz, M. J., Sicard, M., Román, R., Benavent-Oltra, J. A., Barragán, R., Brogniez, G., Denjean, C., Mallet, M., Formenti, P., Torres, B., and Alados-Arboledas, L.: Impact of mineral dust on shortwave and longwave radiation: evaluation of different vertically resolved parameterizations in 1-D radiative transfer computations, *Atmos. Chem. Phys.*, 19, 523–542, <https://doi.org/10.5194/acp-19-523-2019>, 2019.
- 715 Granados-Muñoz, M.J., Benavent-Oltra, J.A., Pérez-Ramírez, D., Lyamani, H., Guerrero-Rascado, J.L., Bravo-Aranda, J.A., Navas-Guzmán, F., Valenzuela, A., Olmo, F.J., Alados-Arboledas, L. Evaluation of LIRIC algorithm performance using independent sun-sky photometer data at two altitude levels *Remote Sensing*, 12 (5), art. no. 842, <https://www.mdpi.com/2072-4292/12/5/842>, 2020.
- 720 Guerrero-Rascado, J. L., Ruiz, B., and Alados Arboledas, L.: Multispectral Lidar characterization of the vertical structure of Saharan dust aerosol over southern Spain, *Atmos. Environ.*, 42, 2668–2681, <https://doi.org/10.1016/j.atmosenv.2007.12.062>, 2008.
- Guerrero-Rascado, J. L., Olmo, F. J., Avilés-Rodríguez, I., Navas-Guzmán, F., Pérez-Ramírez, D., Lyamani, H., and Alados Arboledas, L.: Extreme Saharan dust event over the southern Iberian Peninsula in september 2007: active and passive remote sensing from surface and satellite, *Atmos. Chem. Phys.*, 9, 8453–8469, doi:10.5194/acp-9-8453-2009, 2009.
- 725 Herreras, M., Román, R., Cazorla, A., Toledano, C., Lyamani, H., Torres, B., Cachorro, V.E., Olmo, F.J., Alados-Arboledas, L. and de Frutos, A.M.: Evaluation of retrieved aerosol extinction profiles using as reference the aerosol optical depth differences between various heights, *Atmospheric Research*, 230, <https://doi.org/10.1016/j.atmosres.2019.104625>, 2019.
- 730 Holben, B. N., Eck, T. F., Slutsker, I., Tanre, D., Buis, J. P., Setzer, A., Vermote, E., Reagan, J. A., Kaufman, Y. J., Nakajima, T., Lavenu, F., Jankowiak, I., and Smirnov, A.: AERONET-a federated instrument network a data archive for aerosol characterization, *Remote Sens. Environ.*, 66, 1–16, 1998.
- Horvath, H., Alados Arboledas, L., and Olmo Reyes, F. J.: Angular scattering of the Sahara dust aerosol, *Atmos. Chem. Phys.*, 18, 17735–17744, <https://doi.org/10.5194/acp-18-17735-2018>, 2018.
- 735 IPCC: Contribution of Working Group I to the Fifth Assessment Report of the Intergovernmental Panel on Climate Change, Summary for Policymakers in Climate Change, Stocker, Cambridge University Press, Cambridge, 2013.
- Klett, J. D.: Stable analytical inversion solution for processing lidar returns, *Appl. Optics*, 20, 211–220, 1981.
- 740 Li, L., O. Dubovik, Y. Derimian, G. L. Schuster, T. Lapyonok, P. Litvinov, F. Ducos, D. Fuertes, C. Chen, Z. Li, A. Lopatin, B. Torres and H. Che, “Retrieval of aerosol components directly from satellite and ground-based measurements”, *Atmos. Chem. Phys.* 19, 13409–13443, <https://doi.org/10.5194/acp-19-13409-2019>, 2019.
- Li, L., H. Che, Y. Derimian, O. Dubovik, G. Schuster, C. Chen, Q. Lid, Y. Wang, B. Guo and X. Zhang, “Retrievals of fine mode light-absorbing carbonaceous aerosols from POLDER/PARASOL observations over East and South Asia”, *Remote Sens. Environ.*, 247, Article Number: 111913, DOI: 10.1016/j.rse.2020.111913, 2020.
- 745 Lopatin, A., Dubovik, O., Chaikovskiy, A., Goloub, P., Lapyonok, T., Tanré, D., and Litvinov, P.: Enhancement of aerosol characterization using synergy of lidar and sun-photometer coincident observations: the GARRLiC algorithm, *Atmos. Meas. Tech.*, 6, 2065–2088, <https://doi.org/10.5194/amt-6-2065-2013>, 2013.
- 750 Lyamani, H., Olmo, F. J., and Alados-Arboledas, L.: Physical and optical properties of aerosols over an urban location in Spain: seasonal and diurnal variability, *Atmos. Chem. Phys.*, 10, 239–254, <https://doi.org/10.5194/acp-10-239-2010>, 2010.
- Mallet, M., Dulac, F., Formenti, P., Nabat, P., Sciare, J., Roberts, G., Pelon, J., Ancellet, G., Tanré, D., Parol, F., Denjean, C., Brogniez, G., di Sarra, A., Alados-Arboledas, L., Arndt, J., Auriol, F., Blarel, L., Bourrienne, T., Chazette, P., Chevaillier, S., Claeys, M., D’Anna, B., Derimian, Y., Desboeufs, K., Di Iorio, T., Doussin, J.-F., Durand, P., Féron, A., Freney, E., Gaimoz, C., Goloub, P., Gómez-Amo, J. L., Granados-Muñoz, M. J., Grand, N., Hamonou, E., Jankowiak, I., Jeannot, M., Léon, J.-F., Maillé, M., Mailler, S., Meloni, D., Menut, L., Mombouisse, G., Nicolas, J., Podvin, T., Pont, V., Rea, G., Renard, J.-B., Roblou, L., Schepanski, K., Schwarzenboeck, A., Sellegri, K., Sicard, M., Solmon, F., Somot, S., Torres, B., Totems, J., Triquet, S., Verdier, N., Verwaerde, C., Waquet, F., Wenger, J., and Zapf, P.: Overview of the Chemistry-Aerosol Mediterranean Experiment/Aerosol Direct Radiative Forcing on the Mediterranean Climate (ChArMEX/ADRIMED) summer 2013 campaign, *Atmos. Chem. Phys.*, 16, 455–504, <https://doi.org/10.5194/acp-16-455-2016>, 2016.



- Müller, D., Wandinger, U., and Ansmann, A.: Microphysical particle parameters from extinction and backscatter lidar data by inversion with regularization: simulation, *Appl. Opt.* **38**, 2358–2368, 1999.
- 765 Müller, D., Ansmann, A., Mattis, I., Tesche, M., Wandinger, U., Althausen, D., and Pisani, G.: Aerosol-type-dependent lidar ratios observed with Raman lidar, *J. Geophys. Res.-Atmos.*, **112**, D16202, doi:10.1029/2006jd008292, 2007.
- Müller, T., Laborde, M., Kassell, G., and Wiedensohler, A.: Design and performance of a three-wavelength LED-based total scatter and backscatter integrating nephelometer, *Atmospheric Measurement Techniques*, **4**, 1291–1303, 2011.
- 770 Navas-Guzmán, F., Bravo-Aranda, J. A., Guerrero-Rascado, J. L., Granados-Muñoz, M. J., and Alados-Arboledas, L.: Statistical analysis of aerosol optical properties retrieved by Raman lidar over Southeastern Spain, *Tellus B*, **65**, 21234, <https://doi.org/10.3402/tellusb.v65i0.21234>, 2013.
- Navas-Guzmán, F., Fernández-Gálvez, J., Granados-Muñoz, M. J., Guerrero-Rascado, J. L., Bravo-Aranda, J. A., and Alados-Arboledas, L.: Tropospheric water vapour and relative humidity profiles from lidar and microwave radiometry, *Atmos. Meas. Tech.*, **7**, 1201–1211, <https://doi.org/10.5194/amt-7-1201-2014>, 2014.
- 775 Ortiz-Amezcu, P., Guerrero-Rascado, J. L., Granados-Muñoz, M. J., Benavent-Oltra, J. A., Böckmann, C., Samaras, S., Stachlewska, I. S., Janicka, Ł., Baars, H., Bohlmann, S., and Alados-Arboledas, L.: Microphysical characterization of long-range transported biomass burning particles from North America at three EARLINET stations, *Atmos. Chem. Phys.*, **17**, 5931–5946, <https://doi.org/10.5194/acp-17-5931-2017>, 2017.
- 780 Ortiz-Amezcu, P., Bedoya-Velásquez, A. E., Benavent-Oltra, J. A., Pérez-Ramírez, D., Veselovskii, I., Castro-Santiago, M., Bravo-Aranda, J. A., Guedes, A., Guerrero-Rascado, J. L., and Alados-Arboledas, L.: Implementation of UV rotational Raman channel to improve aerosol retrievals from multiwavelength lidar, *Opt. Express* **28**, 8156–8168, <https://doi.org/10.1364/OE.383441>, 2020.
- Pappalardo, G., Amodeo, A., Apituley, A., Comeron, A., Freudenthaler, V., Linné, H., Ansmann, A., Bösenberg, J., D'Amico, G., Mattis, I., Mona, L., Wandinger, U., Amiridis, V., Alados-Arboledas, L., Nicolae, D., and Wiegner, M.: EARLINET: towards an advanced sustainable European aerosol lidar network, *Atmos. Meas. Tech.*, **7**, 2389–2409, <https://doi.org/10.5194/amt-7-2389-2014>, 2014.
- Pérez-Ramírez, D., Lyamani, H., Olmo, F. J., Whiteman, D. N., and Alados-Arboledas, L.: Columnar aerosol properties from sun-and-star photometry: statistical comparisons and day-to-night dynamic, *Atmos. Chem. Phys.*, **12**, 9719–9738, <https://doi.org/10.5194/acp-12-9719-2012>, 2012.
- 790 Pérez-Ramírez, D., Lyamani, H., Smirnov, A., O'Neill, N. T., Veselovskii, I., Whiteman, D. N., Olmo, F. J., Alados-Arboledas, L.: Statistical study of day and night hourly patterns of columnar aerosol properties using sun and star photometry, *Proc. SPIE*, 100001, 100010K, 2016.
- Pérez-Ramírez, D., Whiteman, D. N., Veselovskii, I., Colarco, P., Korenski, M., and da Silva, A.: Retrievals of aerosol single scattering albedo by multiwavelength lidar measurements: Evaluations with NASA Langley HSRL-2 during discover-AQ field campaigns, *Remote Sens. Environ.*, **222**, 144–164, 2019.
- Román, R., Cazorla, A., Toledano, C., Olmo, F. J., Cachorro, V. E., de Frutos, A., Alados-Arboledas, L.: Cloud cover detection combining high dynamic range sky images and ceilometer measurements. *Atmos. Res.* **196**, 224–236, <https://doi.org/10.1016/j.atmosres.2017.06.006>, 2017.
- 800 Román, R., J. A. Benavent-Oltra, J. A. Casquero-Vera, A. Lopatin, A. Cazorla, H. Lyamani, C. Denjean, D. Fuertes, D. Pérez-Ramírez, B. Torres, C. Toledano, O. Dubovik, V. E. Cachorro, Á. de Frutos, F. J. Olmo, and L. Alados-Arboledas: Retrieval of aerosol profiles combining sun photometer and ceilometer measurements in GRASP code, *Atmospheric Research*, **204**, 161–177, <https://doi.org/10.1016/j.atmosres.2018.01.021>, 2018.
- 805 Román, R., González, R., Toledano, C., Barreto, Á., Pérez-Ramírez, D., Benavent-Oltra, J. A., Olmo, F. J., Cachorro, V. E., Alados-Arboledas, L., and de Frutos, Á. M.: Correction of a lunar-irradiance model for aerosol optical depth retrieval and comparison with a star photometer, *Atmos. Meas. Tech.*, **13**, 6293–6310, <https://doi.org/10.5194/amt-13-6293-2020>, 2020.
- Rose, T., Crewell, S., Löhnert, U., and Simmer, C.: A network suitable microwave radiometer for operational monitoring of the cloudy atmosphere, *Atmos. Res.*, **75**, 183–200, 2005.
- 810 Russell, P. B., Bergstrom, R. W., Shinozuka, Y., Clarke, A. D., DeCarlo, P. F., Jimenez, J. L., Livingston, J. M., Redemann, J., Dubovik, O., and Strawa, A.: Absorption Angstrom Exponent in AERONET and related data as an indicator of aerosol composition, *Atmos. Chem. Phys.*, **10**, 1155–1169, <https://doi.org/10.5194/acp-10-1155-2010>, 2010.
- 815 Shin, S.-K., Tesche, M., Kim, K., Kezoudi, M., Tatarov, B., Müller, D., and Noh, Y.: On the spectral depolarisation and lidar ratio of mineral dust provided in the AERONET version 3 inversion product, *Atmos. Chem. Phys.*, **18**, 12735–12746, <https://doi.org/10.5194/acp-18-12735-2018>, 2018.



- 820 Sicard, M., Granados-Muñoz, M.J., Alados-Arboledas, L., Barragán, R., Bedoya-Velásquez, A.E., Benavent-Oltra, J.A., Bortoli, D., Comerón, A., Córdoba-Jabonero, C., Costa, M.J., del Águila, A., Fernández, A.J., Guerrero-Rascado, J.L., Jorba, O., Molero, F., Muñoz-Porcar, C., Ortiz-Amezcu, P., Papagiannopoulos, N., Potes, M., Pujadas, M., Rocadenbosch, F., Rodríguez-Gómez, A., Román, R., Salgado, R., Salgueiro, V., Sola, Y., Yela, M.: Ground/space, passive/active remote sensing observations coupled with particle dispersion modelling to understand the inter-continental transport of wildfire smoke plumes. *Remote Sensing of Environment*. 232. <https://doi.org/10.1016/j.rse.2019.111294>, 2019.
- 825 Sinyuk, A., Holben, B. N., Eck, T. F., Giles, D. M., Slutsker, I., Korkin, S., Schafer, J. S., Smirnov, A., Sorokin, M., and Lyapustin, A.: The AERONET Version 3 aerosol retrieval algorithm, associated uncertainties and comparisons to Version 2, *Atmos. Meas. Tech.*, 13, 3375–3411, <https://doi.org/10.5194/amt-13-3375-2020>, 2020.
- 830 Sorribas, M., Olmo, F.J., Quirantes, A., Lyamani, H., Gil-Ojeda, M., Alados-Arboledas, L., Horvath, H.: Role of spheroidal particles in closure studies for aerosol microphysical-optical properties. *Quarterly Journal of the Royal Meteorological Society*. 141 - 692, pp. 2700 -2707, 2015.
- Tanré, D., Haywood, J., Pelon, J., Léon, J. F., Chatenet, B., Formenti, P., Francis, P., Goloub, P., Highwood, E. J., Myhre, G.: Measurements and modeling of the Saharan dust radiative impact: overview of the Saharan Dust Experiment (SHADE). *J. Geophys. Res.* 108, doi:10.1029/2002JD003273, 2003.
- 835 Titos, G., Ealo, M., Román, R., Cazorla, A., Sola, Y., Dubovik, O., Alastuey, A., and Pandolfi, M.: Retrieval of aerosol properties from ceilometer and photometer measurements: long-term evaluation with in situ data and statistical analysis at Montsec (southern Pyrenees), *Atmos. Meas. Tech.*, 12, 3255–3267, <https://doi.org/10.5194/amt-12-3255-2019>, 2019.
- 840 Torres, B., Dubovik, O., Fuertes, D., Schuster, G., Cachorro, V. E., Lapyonok, T., Goloub, P., Blarel, L., Barreto, A., Mallet, M., Toledano, C., and Tanré, D.: Advanced characterisation of aerosol size properties from measurements of spectral optical depth using the GRASP algorithm, *Atmos. Meas. Tech.*, 10, 3743–3781, <https://doi.org/10.5194/amt-10-3743-2017>, 2017.
- 845 Tsekeri, A., Lopatin, A., Amiridis, V., Marinou, E., Iglhoffstein, J., Siomos, N., Solomos, S., Kokkalis, P., Engelmann, R., Baars, H., Gratesea, M., Raptis, P. I., Binietoglou, I., Mihalopoulos, N., Kalivitis, N., Kouvarakis, G., Bartsotas, N., Kallos, G., Basart, S., Schuettmeyer, D., Wandinger, U., Ansmann, A., Chaikovsky, A. P., and Dubovik, O.: GARRLiC and LIRIC: strengths and limitations for the characterization of dust and marine particles along with their mixtures, *Atmos. Meas. Tech.*, 10, 4995–5016, <https://doi.org/10.5194/amt-10-4995-2017>, 2017.
- 850 Turco, M., Jerez, S., Augusto, S., Tarín-Carrasco, P., Ratola, N., Jiménez-Guerrero, P. and Trigo R. M.: Climate drivers of the 2017 devastating fires in Portugal. *Sci Rep* 9, 13886, <https://doi.org/10.1038/s41598-019-50281-2>, 2019.
- Valenzuela, A., Olmo, F.J., Lyamani, H., Antón, M., Quirantes, A., Alados-Arboledas, L.: Analysis of the desert dust radiative properties over Granada using principal plane sky radiances and spheroids retrieval procedure. *Atmos. Res.* 104–105, 292–301, <https://doi.org/10.1016/j.atmosres.2011.11.005>, 2012.
- 855 Valenzuela, A., Olmo, F. J., Lyamani, H., Antón, M., Titos, G., Cazorla, A., and Alados-Arboledas, L.: Aerosol scattering and absorption Angström exponents as indicators of dust and dust-free days over Granada (Spain), *Atmos Res.*, 154, 1–13, <https://doi.org/10.1016/j.atmosres.2014.10.015>, 2015.
- Vandenbussche, S., Callewaert, S., Schepanski, K., and De Mazière, M.: North African mineral dust sources: new insights from a combined analysis based on 3D dust aerosol distributions, surface winds and ancillary soil parameters, *Atmos. Chem. Phys.*, 20, 15127–15146, <https://doi.org/10.5194/acp-20-15127-2020>, 2020.
- 860 Veselovskii, I., Kolgotin, A., Griaznov, V., Muller, D., Wandinger, U., Whiteman, D.: Inversion with regularization for the retrieval of tropospheric aerosol parameters from multiwavelength lidar sounding. *Applied Optics*, 41, 3685–3699, 2002.
- 865 Veselovskii, I., Whiteman, D. N., Korenskiy, M., Suvorina, A., and Pérez-Ramírez, D.: Use of rotational Raman measurements in multiwavelength aerosol lidar for evaluation of particle backscattering and extinction, *Atmos. Meas. Tech.*, 8, 4111–4122, <https://doi.org/10.5194/amt-8-4111-2015>, 2015.
- 870 Veselovskii, I., Goloub, P., Podvin, T., Bovchaliuk, V., Derimian, Y., Augustin, P., Fourmentin, M., Tanre, D., Korenskiy, M., Whiteman, D. N., Diallo, A., Ndiaye, T., Kolgotin, A., and Dubovik, O.: Retrieval of optical and physical properties of African dust from multiwavelength Raman lidar measurements during the SHADOW campaign in Senegal, *Atmos. Chem. Phys.*, 16, 7013–7028, <https://doi.org/10.5194/acp-16-7013-2016>, 2016.
- Whiteman, D. N., Melfi, S. H., and Ferrare, R. A.: Raman lidar system for the measurement of water vapor and aerosols in the Earth's atmosphere, *Appl. Optics*, 31, 3068–3082, 1992.



- 875 Wiedensohler, A., Birmili, W., Nowak, A., Sonntag, A., Weinhold, K., Merkel, M., Wehner, B., Tuch, T., Pfeifer, S., Fiebig, M., Fjåraa, A. M., Asmi, E., Sellegri, K., Depuy, R., Venzac, H., Villani, P., Laj, P., Aalto, P., Ogren, J. A., Swietlicki, E., Williams, P., Roldin, P., Quincey, P., Hüglin, C., Fierz-Schmidhauser, R., Gysel, M., Weingartner, E., Riccobono, F., Santos, S., Grüning, C., Faloon, K., Beddows, D., Harrison, R., Monahan, C., Jennings, S. G., O'Dowd, C. D., Marinoni, A., Horn, H.-G., Keck, L., Jiang, J., Scheckman, J., McMurry, P. H., Deng, Z., Zhao, C. S., Moerman, M., Henzing, B., de Leeuw, G., Lösschau, G., and Bastian, S.: Mobility particle size spectrometers: harmonization of technical standards and data structure to facilitate high quality
- 880 long-term observations of atmospheric particle number size distributions, *Atmos. Meas. Tech.*, 5, 657–685, <https://doi.org/10.5194/amt-5-657-2012>, 2012.
- Wiedensohler, A., Wiesner, A., Weinhold, K., Birmili, W., Hermann, M., Merkel, M., Müller, T., Pfeifer, S., Schmidt, A., and Tuch, T.: Mobility particle size spectrometers: Calibration procedures and measurement uncertainties, *Aerosol Sci. Technol.*, 52, 146–164, 2018
- 885 Yus-Díez, J., Ealo, M., Pandolfi, M., Perez, N., Titos, G., Močnik, G., Querol, X., and Alastuey, A.: Aircraft vertical profiles during summertime regional and Saharan dust scenarios over the north-western Mediterranean Basin: aerosol optical and physical properties, *Atmos. Chem. Phys. Discuss.*, <https://doi.org/10.5194/acp-2020-837>, in review, 2020.



890 Table 1. Instruments deployed during SLOPE I and II campaigns at AGORA stations.

Instrument	Location	Measurement variable	Wavelength (nm) / Nominal size range (μm)
Raman lidar system	UGR station	Elastic backscattered signal	355, 532 and 1064 nm
Sun-sky photometer	UGR, CP and SNS stations	Aerosol optical depth and sky radiances	440, 675, 870 and 1020 nm
Nephelometer TSI 3563	SNS station	Scattering coefficient	450, 550, 700 nm
Nephelometer Aurora Ecotech	Aircraft		450, 525, 635 nm
Aethalometer AE-33	SNS station	Absorption coefficient	370, 470, 520, 590, 660, 880 and 950 nm
Aethalometer AVIO AE-33	Aircraft		
Scanning mobility particle sizer, TSI 3082	SNS station	Aitken + accumulation mode conc.	0.012 – 0.615 μm
Aerodynamic Particle Sizer, TSI 3321	SNS station	Coarse mode conc.	0.5 – 20 μm

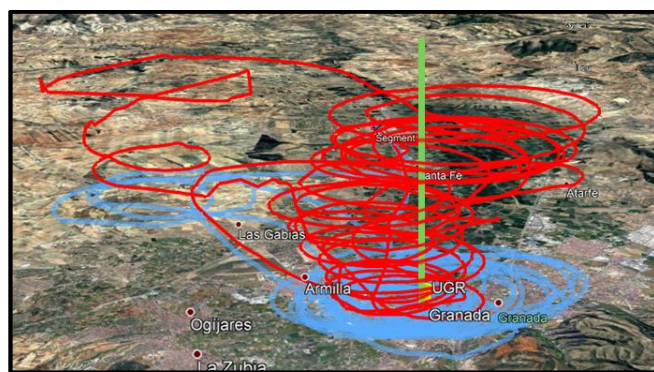
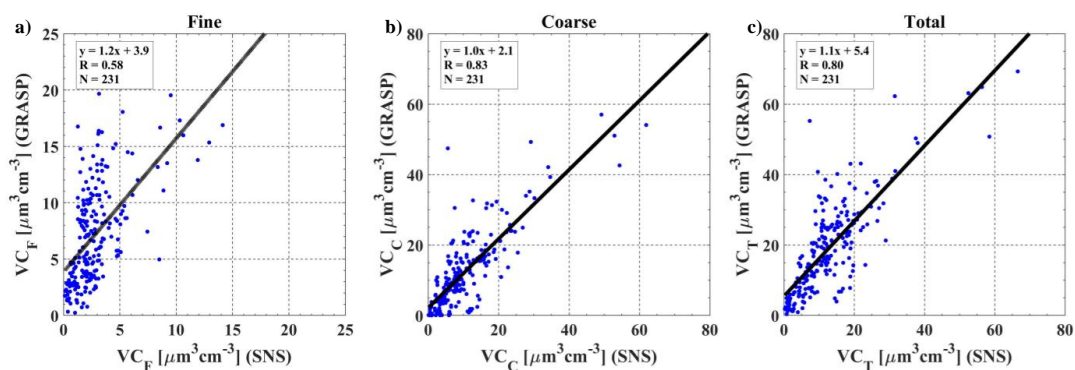
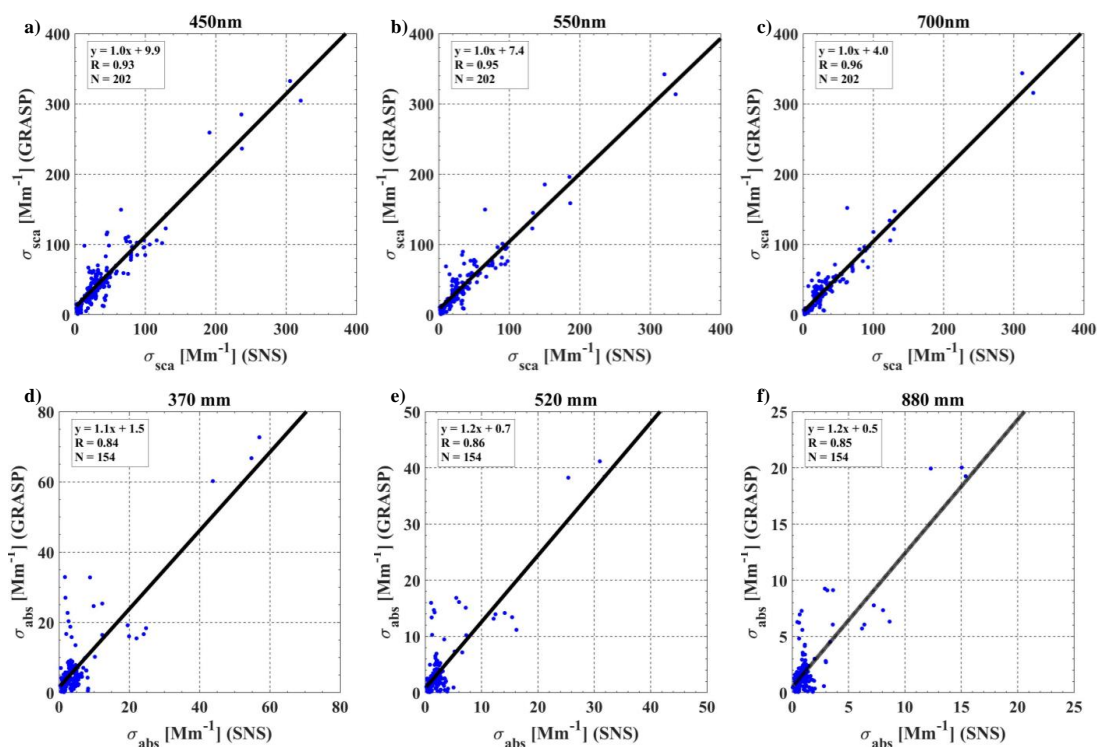


Figure 1. Map illustrating UGR station. The blue and red lines indicate the trajectories of the aircraft during SLOPE I campaign. The red line indicates the vertical of lidar measurements. © Google Earth

895



900 Figure 2. Volume concentration (VC) retrieved by GRASP at SNS height versus in-situ measurements at SNS for (a) fine, (b) coarse and (c) total modes.



905 Figure 3. (a, b, c) Scattering (σ_{sca}) and (d, e, f) absorption (σ_{abs}) coefficients retrieved by GRASP at SNS height versus in-situ measurements at SNS.



910

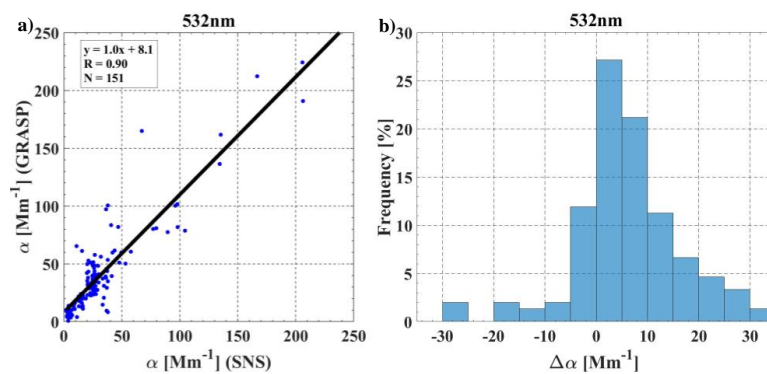


Figure 4. (a) Extinction (α) coefficient retrieved by GRASP at SNS height versus the in-situ measurements at SNS and (b) the histogram of the absolute difference between GRASP and SNS in-situ measurements.

915

920

925

930

935

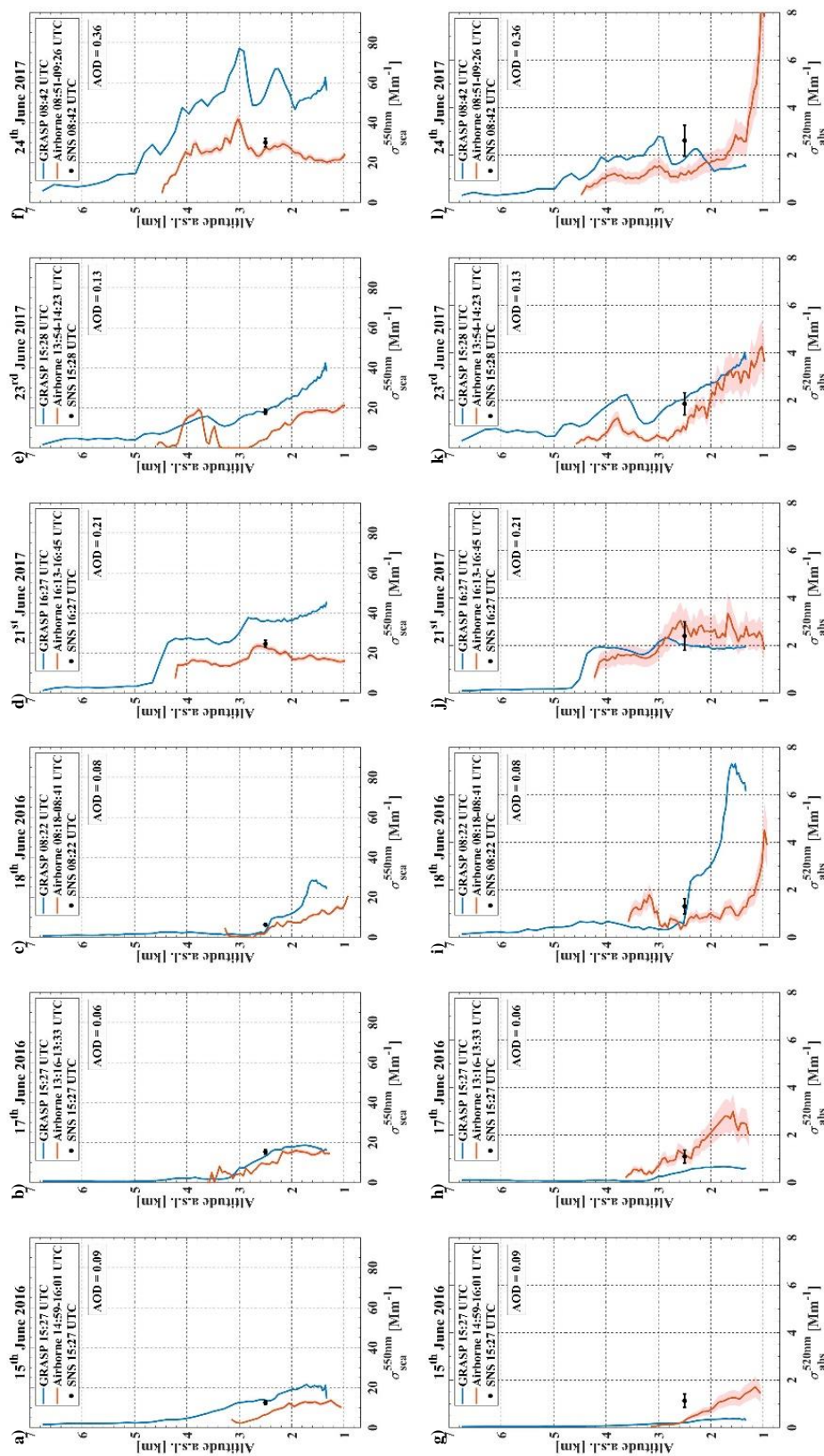


Figure 5. Scattering (σ_{scat}) and absorption (σ_{abs}) coefficients at 520 nm retrieved by GRASP (blue), aircraft (red) and SNS (black) in-situ measurements on (a, g) 15th, (b, h) 17th and (c, i) 18th June 2016 and (d, j) 21st, (e, k) 23rd and (f, l) 24th June 2017. The AOD showed is at 440 nm.

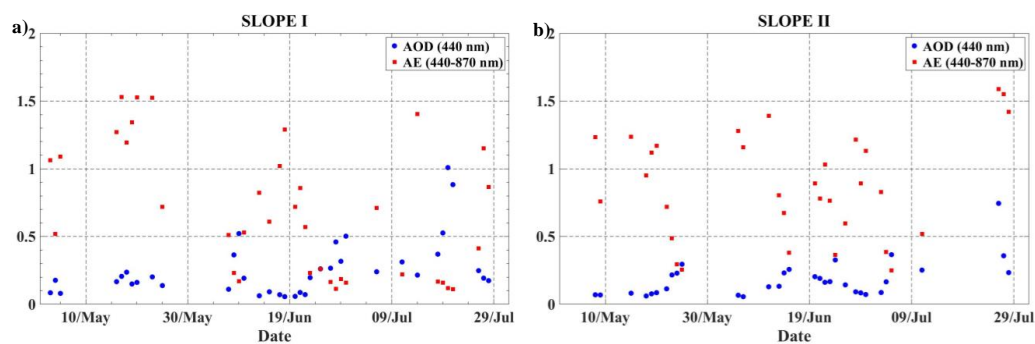
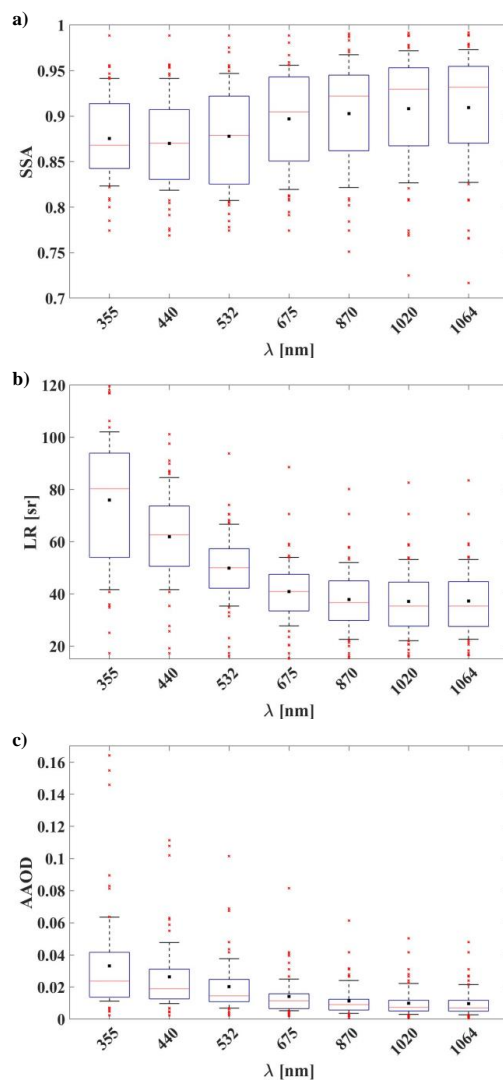


Figure 6. Temporal evolution of aerosol optical depth (AOD) at 440 nm and Ångström exponent (440–870 nm) retrieved by GRASP during (a) SLOPE I and (b) SLOPE II campaigns.

945



950



955

Figure 7. Statistics of (a) single-scattering albedo (SSA), (b) lidar ratio (LR) and (c) absorption aerosol optical depth (AAOD), at 355, 440, 532, 675, 870, 1020 and 1064 nm retrieved by GRASP code during SLOPE I and II campaigns represented as box diagrams. In these box diagrams, the mean is represented by a black dot and the line segment in the box is the median. The bottom and top edges of the box indicate the 25th and 75th percentiles, respectively. In addition, the error bars of the box are the 10th and 90th percentiles, and the crosses represent the outliers values.

960

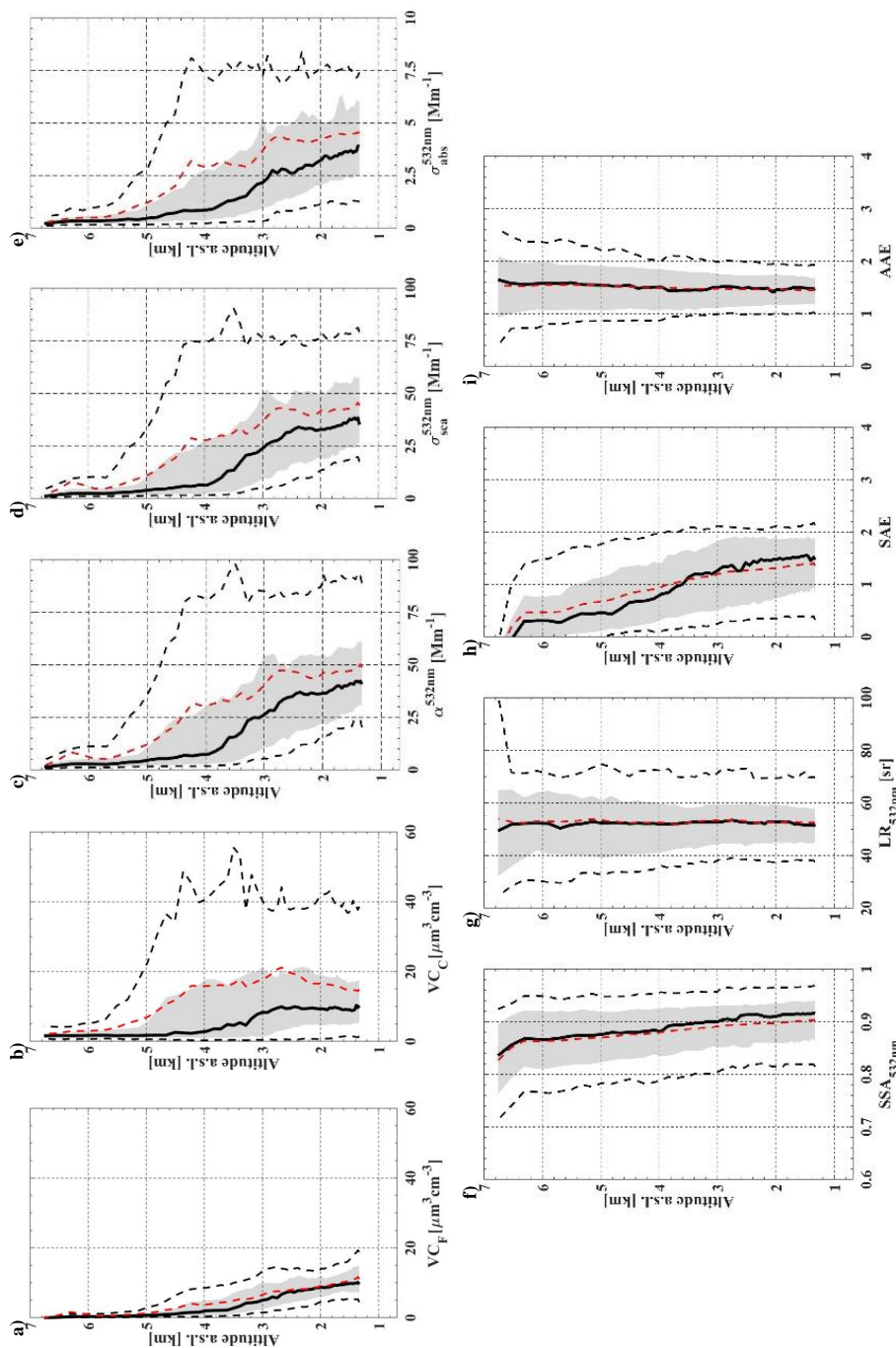
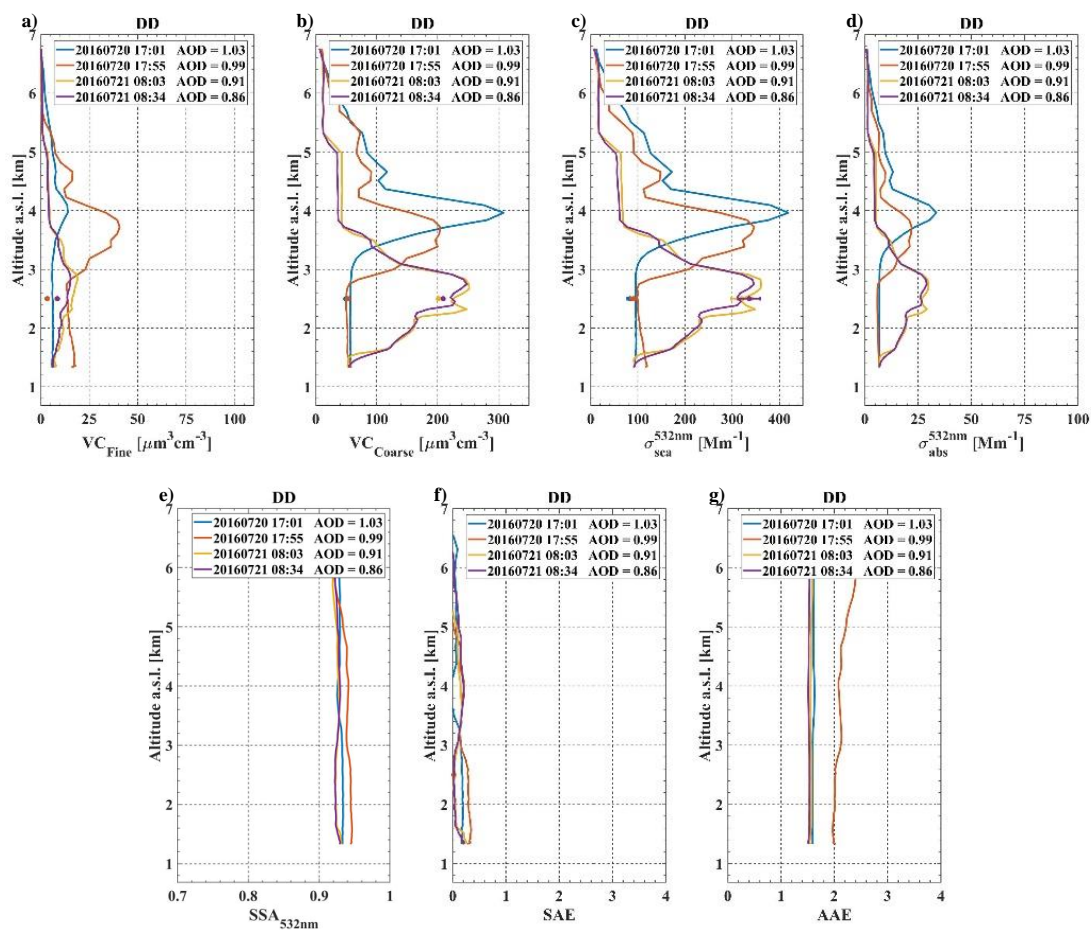
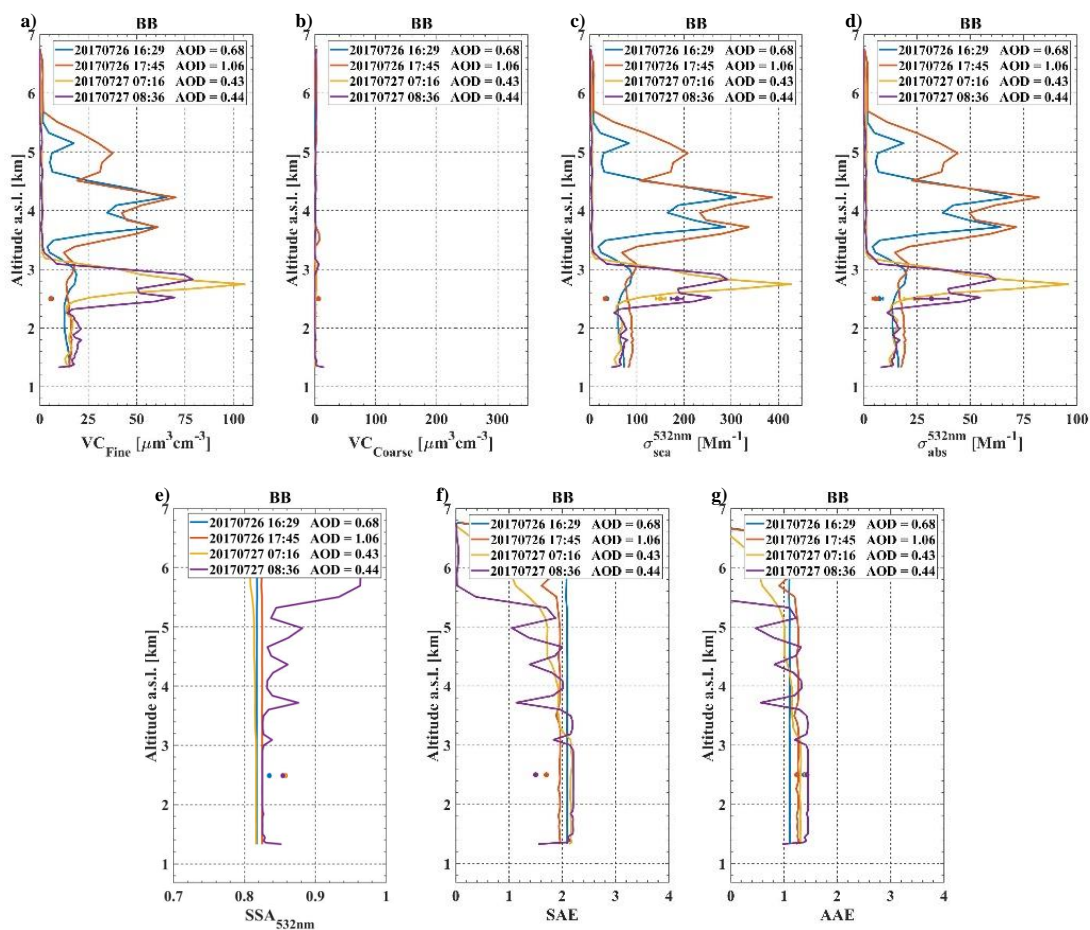


Figure 8. Variability of GRASP vertical profiles: volume concentration for (a) fine and (b) coarse modes; (c) scattering (σ_{sca}) and (e) absorption (σ_{abs}) coefficients; (f) single-scattering albedo (SSA) and (g) lidar ratio (LR) at 532 nm; (h) scattering Angström exponent (SAE) and (i) absorption Angström exponent (AAE) computed between 355 and 1064 nm. The black line represents the median and the red dashed line is the 10th and 90th percentiles. The shadowed area is the interquartile range and the black dashed lines represent the 10th and 90th percentiles. Statistics are based on daily average profiles.



970

Figure 9. Volume concentration for (a) fine and (b) coarse modes, (c) scattering (σ_{sea}) and (d) absorption (σ_{abs}) coefficients, (e) single scattering albedo (SSA) at 532 nm, (f) scattering Ångström exponent (SAE) and (g) absorption Ångström exponent (AAE) retrieved by GRASP (line) and SNS measurements (point) during desert dust event on 20th and 21st July 2016. The AOD showed is at 440 nm.



975

Figure 10. Volume concentration for (a) fine and (b) coarse modes, (c) scattering (σ_{sca}) and (d) absorption (σ_{abs}) coefficients, (e) single scattering albedo (SSA) at 532 nm, (f) scattering Ångström exponent (SAE) and (g) absorption Ångström exponent (AAE) retrieved by GRASP (line) and SNS measurements (point) during biomass burning event on 26th and 27th July 2017. The AOD showed is at 440 nm.

980

985

990